

Non-linear exact geometry 12-node solid-shell element with three translational degrees of freedom per node

G. M. Kulikov^{*,†} and S. V. Plotnikova

*Department of Applied Mathematics and Mechanics, Tambov State Technical University,
Sovetskaya Street, 106, Tambov 392000, Russia*

SUMMARY

This paper presents the finite rotation exact geometry (EG) 12-node solid-shell element with 36 displacement degrees of freedom. The term 'EG' reflects the fact that coefficients of the first and second fundamental forms of the reference surface and Christoffel symbols are taken exactly at each element node. The finite element formulation developed is based on the 9-parameter shell model by employing a new concept of sampling surfaces (S-surfaces) inside the shell body. We introduce three S-surfaces, namely, bottom, middle and top, and choose nine displacements of these surfaces as fundamental shell unknowns. Such choice allows one to represent the finite rotation higher order EG solid-shell element formulation in a very compact form and to derive the strain–displacement relationships, which are objective, that is, invariant under arbitrarily large rigid-body shell motions in convected curvilinear coordinates. The tangent stiffness matrix is evaluated by using 3D analytical integration and the *explicit* presentation of this matrix is given. The latter is unusual for the non-linear EG shell element formulation. Copyright © 2011 John Wiley & Sons, Ltd.

Received 3 October 2010; Revised 4 March 2011; Accepted 14 April 2011

KEY WORDS: 9-parameter shell model; finite rotation; exact geometry shell element, 12-node solid-shell element

1. INTRODUCTION

A large number of works has been carried out to develop the finite rotation higher order shell formulation with thickness stretching. These works are devoted, as a rule, to the 7-parameter shell theory [1–9] in which the transverse normal strain varies at least linearly through the shell thickness. This fact is of great importance since the popular 6-parameter shell formulation based on the complete 3D constitutive equations exhibits thickness locking. The errors caused by thickness locking do not decrease with the mesh refinement because the reason of stiffening lies in the shell theory itself rather than the finite element discretization. To prevent thickness locking, the 3D constitutive equations have to be modified employing generalized plane stress conditions [10–15]. However, the use of complete 3D constitutive laws within the shell analysis is of great importance for engineering applications. In this aspect, the advanced finite element techniques were developed, namely, a hybrid stress method [16] in which the transverse normal stress is constant through the thickness and a most popular enhanced assumed strain method in which the transverse normal strain is enriched in the thickness direction by a linear term [17, 18].

^{*}Correspondence to: G. M. Kulikov, Department of Applied Mathematics and Mechanics, Tambov State Technical University, Sovetskaya Street, 106, Tambov 392000, Russia.

[†]E-mail: kulikov@apmath.tstu.ru

It is well known that a conventional way for developing the higher order shell theory is to utilize either quadratic or cubic series expansions in the thickness coordinate and to choose as unknowns the generalized displacements of the midsurface. Herein, the 9-parameter shell model is developed using a new concept of sampling surfaces (S-surfaces) inside the shell body [7, 19, 20]. We choose three equally located S-surfaces, namely, bottom, middle and top, and introduce displacement vectors of these surfaces as fundamental shell unknowns. Such choice of displacements with the consequent use of Lagrange polynomials of degree two in the thickness direction permits one to represent the finite rotation higher order 9-parameter shell formulation in a very compact form and to derive non-linear strain–displacement relationships, which are invariant under arbitrarily large rigid-body shell motions. Taking into account that displacement vectors of S-surfaces are resolved in the reference surface frame the proposed higher order shell formulation is very promising for developing the high performance EG solid-shell elements. This term means that the parametrization of the reference surface is known and, therefore, coefficients of the first and second fundamental forms and Christoffel symbols are taken exactly at element nodes, which are employed in innovative analytical integration schemes proposed by the authors [7, 15, 21].

To avoid shear and membrane locking and have no spurious zero energy modes, the assumed displacement-independent strains and stress-resultant fields are invoked [22]. This approach was developed for the finite rotation 6- and 7-parameter EG beam, plate and shell element formulations in [7, 9, 23, 24]. Herein, the above hybrid stress–strain formulation is generalized to the finite rotation EG solid-shell element based on the higher order 9-parameter shell theory. The proposed EG solid-shell element formulation has computational advantages compared with conventional isoparametric solid-shell element formulations, since it reduces the computational cost of numerical integration in the evaluation of the tangent stiffness matrix. This is due to the fact that, first, all element matrices require only direct substitutions, i.e. no numerical matrix inversion is needed. The latter is unusual for the isoparametric hybrid/mixed shell element formulation [10, 11, 13, 16]. Second, we employ efficient 3D analytical integration [7, 15, 21] that permits the use of coarser meshes. Finally, the hybrid stress–strain EG solid-shell element developed allows one to utilize load increments, which are much larger than possible with the existing displacement-based EG solid-shell elements [6, 12]. Therefore, large-scale computations for thick shell structures undergoing finite rotations can be carried out efficiently with the help of the proposed EG 12-node solid-shell element in which there are four nodes at each S-surface exactly.

2. KINEMATIC DESCRIPTION OF UNDEFORMED SHELL

Consider a thick shell of the thickness h . The shell can be defined as a 3D body of volume V bounded by two outer surfaces Ω^- and Ω^+ , located at the distances d^- and d^+ measured with respect to the reference surface Ω such that $h = d^- + d^+$, and the edge boundary surface Σ . The reference surface is assumed to be sufficiently smooth and without any singularities. This assumption cannot introduce any serious limitation in the shell theory because in the case of the robust choice of the reference surface we are able to model general surface geometry such as shell intersections and shell edges efficiently [25]. Let the reference surface be referred to the convected curvilinear coordinates θ^1 and θ^2 , whereas the coordinate θ^3 is oriented along the unit vector $\mathbf{a}_3 = \mathbf{a}^3$ normal to the reference surface. As S-surfaces Ω^1 , Ω^2 and Ω^3 , we choose bottom, middle and top surfaces of the shell.

Introduce in accordance with Figures 1 and 2 the following notations: $\mathbf{r} = \mathbf{r}(\theta^1, \theta^2)$ is the position vector of any point of the reference surface; $\mathbf{a}_\alpha = \mathbf{r}_{,\alpha}$ are the covariant base vectors of the reference surface; \mathbf{a}^β are the contravariant base vectors of the reference surface defined by the standard relation $\mathbf{a}_\alpha \cdot \mathbf{a}^\beta = \delta_\alpha^\beta$; $\mathbf{a}_{\alpha\beta} = \mathbf{a}_\alpha \cdot \mathbf{a}_\beta$ and $\mathbf{a}^{\alpha\beta} = \mathbf{a}^\alpha \cdot \mathbf{a}^\beta$ are the covariant and contravariant components of the metric tensor of the reference surface; $a = \det[a_{\alpha\beta}]$ is the determinant of the metric tensor of the reference surface; b_α^β are the mixed components of the curvature tensor defined as $b_\alpha^\beta = -\mathbf{a}^\beta \cdot \mathbf{a}_{3,\alpha}$; \mathbf{R} is the position vector of any point in the shell body given by $\mathbf{R} = \mathbf{r} + \theta^3 \mathbf{a}_3$; in particular, position vectors of S-surfaces are $\mathbf{R}^I = \mathbf{r} + z^I \mathbf{a}_3$, where z^I are the transverse coordinates of S-surfaces

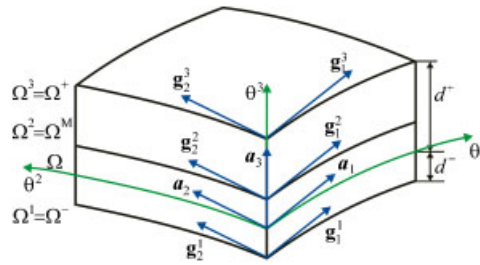


Figure 1. Geometry of the shell.

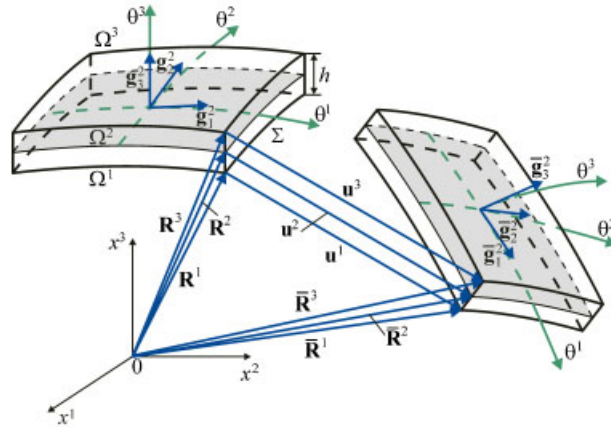


Figure 2. Initial and current configurations of the shell in the case of choosing the midsurface as a reference surface.

defined as

$$z^1 = -d^-, \quad z^2 = (d^+ - d^-)/2, \quad z^3 = d^+, \tag{1}$$

μ_α^β are the mixed components of the 3D shifter tensor expressed as $\mu_\alpha^\beta = \delta_\alpha^\beta - \theta^3 b_\alpha^\beta$; in particular, components of the shifter tensor at S-surfaces are $\mu_\alpha^{I\beta} = \delta_\alpha^\beta - z^I b_\alpha^\beta$; \mathbf{g}_i are the covariant base vectors in the shell body given by

$$\mathbf{g}_\alpha = \mathbf{R}_{,\alpha} = \mu_\alpha^\beta \mathbf{a}_\beta, \quad \mathbf{g}_3 = \mathbf{R}_{,3} = \mathbf{a}_3, \tag{2}$$

in particular, base vectors of S-surfaces are

$$\mathbf{g}_\alpha^I = \mathbf{R}_{,\alpha}^I = \mu_\alpha^{I\beta} \mathbf{a}_\beta, \quad \mathbf{g}_3^I = \mathbf{a}_3, \tag{3}$$

g_{ij} are the covariant components of the 3D metric tensor defined as

$$g_{\alpha\beta} = \mathbf{g}_\alpha \cdot \mathbf{g}_\beta = \mu_\alpha^\gamma \mu_\beta^\delta a_{\gamma\delta}, \quad g_{i3} = \mathbf{g}_i \cdot \mathbf{g}_3 = \delta_{i3}, \tag{4}$$

in particular, components of the metric tensors of S-surfaces are

$$g_{\alpha\beta}^I = \mathbf{g}_\alpha^I \cdot \mathbf{g}_\beta^I = \mu_\alpha^{I\gamma} \mu_\beta^{I\delta} a_{\gamma\delta}, \quad g_{i3}^I = \mathbf{g}_i^I \cdot \mathbf{g}_3^I = \delta_{i3}, \tag{5}$$

$g = \det[g_{ij}]$ is the determinant of the 3D metric tensor; $g^I = \det[g_{ij}^I]$ are the determinants of the metric tensors of S-surfaces; $\mu = \sqrt{g/a}$ is the determinant of the shifter tensor; $\mu^I = \sqrt{g^I/a}$ are the determinants of the shifter tensor at S-surfaces; $(\dots)_{,i}$ are the partial derivatives in V with respect to coordinates θ^i ; $(\dots)|_\alpha$ are the covariant derivatives in Ω with respect to coordinates θ^α .

Here and in the following developments, Greek tensorial indices α, β, γ range from 1 to 2; Latin tensorial indices i, j, m, n range from 1 to 3; indices I, J identify the belonging of any quantity to the S-surfaces and take values 1, 2 and 3.

3. KINEMATIC DESCRIPTION OF DEFORMED SHELL

Let us introduce the first assumption for the proposed higher order shell theory. The displacement field is approximated in the thickness direction according to the quadratic law [19]

$$\mathbf{u} = \sum_I L^I \mathbf{u}^I, \quad (6)$$

where $\mathbf{u}^I(\theta^1, \theta^2)$ are the displacement vectors of S-surfaces; $L^I(\theta^3)$ are the Lagrange polynomials of degree two expressed as

$$\begin{aligned} L^1 &= \frac{2}{h^2}(z^2 - \theta^3)(z^3 - \theta^3), \\ L^2 &= \frac{4}{h^2}(\theta^3 - z^1)(z^3 - \theta^3), \\ L^3 &= \frac{2}{h^2}(\theta^3 - z^1)(\theta^3 - z^2) \end{aligned} \quad (7)$$

such that $L^I(z^J) = 1$ for $J = I$ and $L^I(z^J) = 0$ for $J \neq I$. Thus, we deal with the higher order 9-parameter shell model because nine displacements of S-surfaces are introduced as shell unknowns.

A position vector of the deformed shell is written as

$$\bar{\mathbf{R}} = \mathbf{R} + \mathbf{u}. \quad (8)$$

In particular, position vectors of S-surfaces are

$$\bar{\mathbf{R}}^I = \mathbf{R}^I + \mathbf{u}^I. \quad (9)$$

The covariant base vectors in the current shell configuration are given by

$$\bar{\mathbf{g}}_i = \bar{\mathbf{R}}_{,i} = \mathbf{g}_i + \mathbf{u}_{,i}. \quad (10)$$

In particular, base vectors of S-surfaces of the deformed shell are

$$\begin{aligned} \bar{\mathbf{g}}_\alpha^I &= \bar{\mathbf{R}}_{,\alpha}^I = \mathbf{g}_\alpha^I + \mathbf{u}_{,\alpha}^I, \\ \bar{\mathbf{g}}_3^I &= \bar{\mathbf{g}}_3(z^I) = \mathbf{a}_3 + \boldsymbol{\beta}^I, \end{aligned} \quad (11)$$

where

$$\begin{aligned} \boldsymbol{\beta}^1 &= \mathbf{u}_{,3}(z^1) = \frac{1}{h}(-3\mathbf{u}^1 + 4\mathbf{u}^2 - \mathbf{u}^3), \\ \boldsymbol{\beta}^2 &= \mathbf{u}_{,3}(z^2) = \frac{1}{h}(-\mathbf{u}^1 + \mathbf{u}^3), \\ \boldsymbol{\beta}^3 &= \mathbf{u}_{,3}(z^3) = \frac{1}{h}(\mathbf{u}^1 - 4\mathbf{u}^2 + 3\mathbf{u}^3). \end{aligned} \quad (12)$$

Remark 1

The derivative vectors at S-surfaces $\boldsymbol{\beta}^I$ are linearly dependent since

$$\boldsymbol{\beta}^2 = \frac{1}{2}(\boldsymbol{\beta}^1 + \boldsymbol{\beta}^3). \quad (13)$$

This is because of the fact that the derivative of the displacement vector $\mathbf{u}_{,3}$ varies linearly through the shell thickness. The latter brings the additional difficulties in describing the rotational rigid-body modes as we shall see in Section 9.1.

4. STRAIN-DISPLACEMENT RELATIONSHIPS

The Green-Lagrange strain tensor can be written as

$$2\varepsilon_{ij} = \bar{\mathbf{g}}_i \cdot \bar{\mathbf{g}}_j - \mathbf{g}_i \cdot \mathbf{g}_j. \quad (14)$$

In particular, Green-Lagrange strain components at S-surfaces are

$$2\varepsilon_{ij}^I = 2\varepsilon_{ij}(z^I) = \bar{\mathbf{g}}_i^I \cdot \bar{\mathbf{g}}_j^I - \mathbf{g}_i^I \cdot \mathbf{g}_j^I. \quad (15)$$

Substituting base vectors (11) into strain-displacement relationships (15), one obtains

$$\begin{aligned} 2\varepsilon_{\alpha\beta}^I &= \mathbf{u}_{,\alpha}^I \cdot \mathbf{g}_\beta^I + \mathbf{u}_{,\beta}^I \cdot \mathbf{g}_\alpha^I + \mathbf{u}_{,\alpha}^I \cdot \mathbf{u}_{,\beta}^I, \\ 2\varepsilon_{\alpha 3}^I &= \mathbf{u}_{,\alpha}^I \cdot \mathbf{a}_3 + \boldsymbol{\beta}^I \cdot \mathbf{g}_\alpha^I + \boldsymbol{\beta}^I \cdot \mathbf{u}_{,\alpha}^I, \\ 2\varepsilon_{33}^I &= 2\boldsymbol{\beta}^I \cdot \mathbf{a}_3 + \boldsymbol{\beta}^I \cdot \boldsymbol{\beta}^I. \end{aligned} \quad (16)$$

The following step consists in a choice of correct approximation of strains through the thickness of the shell. It is apparent that the best solution of the problem is to choose the strain distribution, which is similar to the displacement distribution (6), that is

$$\varepsilon_{ij} = \sum_I L^I \varepsilon_{ij}^I. \quad (17)$$

Remark 2

It is necessary to note that the quadratic distribution of the transverse normal strain in the thickness direction permits one to utilize 3D constitutive laws. In principle, the linear strain distribution is sufficient for analysis of thin shell structures [1, 2].

Next, we represent displacement vectors of S-surfaces as follows:

$$\mathbf{u}^I = u_i^I \mathbf{a}^i. \quad (18)$$

It is seen that displacement vectors are resolved in the contravariant reference surface basis \mathbf{a}^i that allows us to reduce the computational cost of numerical integration in the evaluation of the stiffness matrix [7, 9, 12, 25]. The derivative vectors at S-surfaces (12) can be represented in a similar way

$$\boldsymbol{\beta}^I = \beta_i^I \mathbf{a}^i, \quad (19)$$

where

$$\beta_i^1 = \frac{1}{h}(-3u_i^1 + 4u_i^2 - u_i^3), \quad \beta_i^2 = \frac{1}{h}(-u_i^1 + u_i^3), \quad \beta_i^3 = \frac{1}{h}(u_i^1 - 4u_i^2 + 3u_i^3). \quad (20)$$

The derivatives of displacement vectors of S-surfaces with respect to coordinates θ^α are written as

$$\mathbf{u}_{,\alpha}^I = u_i^I |_{\alpha} \mathbf{a}^i, \quad (21)$$

$$u_i^I |_{\alpha} = u_{i,\alpha}^I - \Gamma_{i\alpha}^j u_j^I, \quad (22)$$

where $\Gamma_{i\alpha}^j$ are the Christoffel symbols defined as

$$\Gamma_{\alpha\beta}^i = \mathbf{a}^i \cdot \mathbf{a}_{\alpha,\beta}, \quad \Gamma_{3\alpha}^\beta = -b_{\alpha}^\beta, \quad \Gamma_{3\alpha}^3 = 0. \quad (23)$$

Substituting (3), (19) and (21) into strain-displacement relationships (16), we arrive at a more convenient form of these relationships

$$\begin{aligned} 2\varepsilon_{\alpha\beta}^I &= \mu_\beta^{I\gamma} u_\gamma^I |_{\alpha} + \mu_\alpha^{I\gamma} u_\gamma^I |_{\beta} + a^{ij} u_i^I |_{\alpha} u_j^I |_{\beta}, \\ 2\varepsilon_{\alpha 3}^I &= u_3^I |_{\alpha} + \mu_\alpha^{I\gamma} \beta_\gamma^I + a^{ij} \beta_i^I u_j^I |_{\alpha}, \\ 2\varepsilon_{33}^I &= 2\beta_3^I + a^{ij} \beta_i^I \beta_j^I. \end{aligned} \quad (24)$$

Here, it is accepted $a^{i3} = \delta^{i3}$. In orthogonal curvilinear coordinates, the strain–displacement relationships can be represented in a simpler form (see Appendix A).

Remark 3

The Green–Lagrange strain components (17) are objective, i.e. they represent precisely arbitrarily large rigid-body shell motions in any convected curvilinear coordinate system. A proof of this statement can be derived following a technique developed in [7, 20, 26].

5. HU-WASHIZU VARIATIONAL EQUATION FOR 9-PARAMETER SHELL FORMULATION

A higher order 9-parameter shell theory developed is based on the assumed approximations of displacements (6) and displacement-dependent strains ε_{ij} (17) in the thickness direction. Additionally, to circumvent shear and membrane locking, we introduce the similar approximation for the assumed displacement-independent strains $\hat{\varepsilon}_{ij}$, that is

$$\hat{\varepsilon}_{ij} = \sum_I L^I \hat{\varepsilon}_{ij}^I, \quad (25)$$

where $\hat{\varepsilon}_{ij}^I(\theta^1, \theta^2)$ are the components of the displacement-independent strain tensor at S-surfaces.

For the sake of simplicity, our discussion is limited to the case of linear elastic materials, zero body forces and conservative surface loading. To arrive at the assumed stress–strain element formulation, we consider the Hu–Washizu functional as follows:

$$\begin{aligned} J_{\text{HW}} = & \iint_{\Omega_{\text{el}}} \int_{-d^-}^{d^+} \left[\frac{1}{2} \hat{\varepsilon}_{ij} C^{ijmn} \hat{\varepsilon}_{mn} - S^{ij} (\hat{\varepsilon}_{ij} - \varepsilon_{ij}) \right] \mu \sqrt{a} \, d\theta^1 \, d\theta^2 \, d\theta^3 \\ & - \iint_{\Omega_{\text{el}}} (\mu^3 p_3^i u_i^3 - \mu^1 p_1^i u_i^1) \sqrt{a} \, d\theta^1 \, d\theta^2 - W_{\text{el}}, \end{aligned} \quad (26)$$

where S^{ij} are the contravariant components of the second Piola–Kirchhoff stress tensor; C^{ijmn} are the contravariant components of the material tensor; p_1^i and p_3^i are the contravariant components of traction vectors applied to the bottom and top surfaces; W_{el} is the work done by external loads acting on the edge boundary surface Σ_{el} .

Substituting assumed approximations of displacements and strains in the thickness direction (6), (17) and (25) into the mixed functional (26) and introducing stress resultants

$$H_I^{ij} = \int_{-d^-}^{d^+} \mu S^{ij} L^I \, d\theta^3, \quad (27)$$

and invoking the stationarity of this functional with respect to independent variables, one derives the following mixed variational equation for the 9-parameter EG solid-shell element formulation:

$$\begin{aligned} \sum_I \iint_{\tilde{\Omega}_{\text{el}}} \left[\delta(\hat{\mathbf{E}}^I)^T (\mathbf{H}_I - \sum_J \mathbf{D}_{IJ} \hat{\mathbf{E}}^J) + \delta \mathbf{H}_I^T (\hat{\mathbf{E}}^I - \mathbf{E}^I) - \delta(\mathbf{E}^I)^T \mathbf{H}_I + \delta(\mathbf{u}^I)^T \mathbf{p}_I \right] \sqrt{a} \Lambda \, d\xi^1 \, d\xi^2 \\ + \delta W_{\text{el}} = 0, \end{aligned} \quad (28)$$

where $\tilde{\Omega}_{\text{el}} = [-1, 1] \times [-1, 1]$ is the biunit square in (ξ^1, ξ^2) -space (see Figure 3); $\Lambda = \det(\partial\theta^B / \partial\xi^\alpha)$ is the determinant of the transformation matrix; \mathbf{u}^I , \mathbf{p}_I , \mathbf{E}^I , $\hat{\mathbf{E}}^I$, \mathbf{H}_I are the column matrices; \mathbf{D}_{IJ} are the constitutive stiffness matrices defined as

$$\begin{aligned} \mathbf{u}^I &= [u_1^I \ u_2^I \ u_3^I]^T, \quad \mathbf{p}_1 = [-\mu^1 p_1^1 \ -\mu^1 p_1^2 \ -\mu^1 p_1^3]^T, \\ \mathbf{p}_2 &= [0 \ 0 \ 0]^T, \quad \mathbf{p}_3 = [\mu^3 p_3^1 \ \mu^3 p_3^2 \ \mu^3 p_3^3]^T, \end{aligned}$$

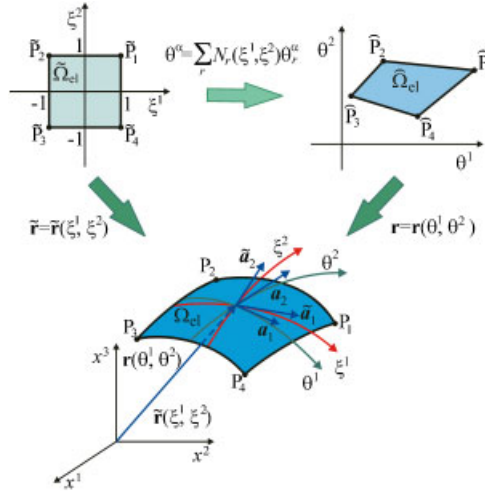


Figure 3. Biunit square in (ξ^1, ξ^2) -space mapped into the reference surface of the EG solid-shell element in (x^1, x^2, x^3) -space.

$$\mathbf{E}^I = [\varepsilon_{11}^I \quad \varepsilon_{22}^I \quad \varepsilon_{33}^I \quad 2\varepsilon_{12}^I \quad 2\varepsilon_{13}^I \quad 2\varepsilon_{23}^I]^T, \quad \hat{\mathbf{E}}^I = [\hat{\varepsilon}_{11}^I \quad \hat{\varepsilon}_{22}^I \quad \hat{\varepsilon}_{33}^I \quad 2\hat{\varepsilon}_{12}^I \quad 2\hat{\varepsilon}_{13}^I \quad 2\hat{\varepsilon}_{23}^I]^T,$$

$$\mathbf{H}_I = [H_I^{11} \quad H_I^{22} \quad H_I^{33} \quad H_I^{12} \quad H_I^{13} \quad H_I^{23}]^T,$$

$$\mathbf{D}_{IJ} = \begin{bmatrix} D_{IJ}^{1111} & D_{IJ}^{1122} & D_{IJ}^{1133} & D_{IJ}^{1112} & 0 & 0 \\ & D_{IJ}^{2222} & D_{IJ}^{2233} & D_{IJ}^{2212} & 0 & 0 \\ & & D_{IJ}^{3333} & D_{IJ}^{3312} & 0 & 0 \\ & & & D_{IJ}^{1212} & 0 & 0 \\ & & & & D_{IJ}^{1313} & D_{IJ}^{1323} \\ \text{sym.} & & & & & D_{IJ}^{2323} \end{bmatrix}, \quad (29)$$

where

$$D_{IJ}^{ijmn} = C^{ijmn} \int_{-d^-}^{d^+} \mu L^I L^J d\theta^3. \quad (30)$$

Recalling that μ and L^I are the polynomials of degree two, one can carry out exact integration in (30) by using the four-point Gaussian quadrature rule.

6. MODIFIED ASSUMED NATURAL STRAIN METHOD

The finite element formulation[‡] is based on the simple and efficient interpolation of shells via *curved* EG 12-node solid-shell elements (Figure 4)

$$\mathbf{v} = \sum_r N_r \mathbf{v}_r, \quad \mathbf{v} = [u_1^1 \quad u_2^1 \quad u_3^1 \quad u_1^2 \quad u_2^2 \quad u_3^2 \quad u_1^3 \quad u_2^3 \quad u_3^3]^T, \quad (31)$$

$$\mathbf{v}_r = [u_{1r}^1 \quad u_{2r}^1 \quad u_{3r}^1 \quad u_{1r}^2 \quad u_{2r}^2 \quad u_{3r}^2 \quad u_{1r}^3 \quad u_{2r}^3 \quad u_{3r}^3]^T,$$

[‡]From this point, we consider just an orthogonal curvilinear coordinate system introduced in Appendix A and a dot over all components of displacement vectors and strain tensors of S-surfaces are omitted.

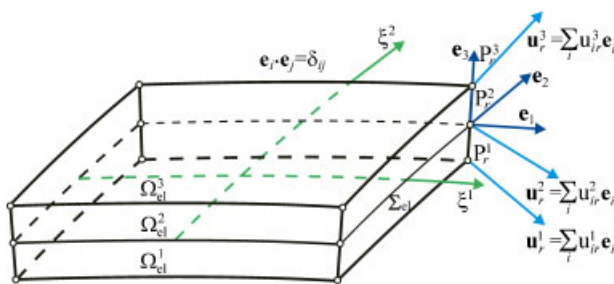


Figure 4. EG 12-node solid-shell element based on the 9-parameter shell model in the case of choosing the midsurface as a reference surface.

$$N_r = \frac{1}{4}(1 + n_{1r}\xi^1)(1 + n_{2r}\xi^2),$$

$$n_{1r} = \begin{cases} 1 & \text{for } r = 1, 4, \\ -1 & \text{for } r = 2, 3, \end{cases} \quad n_{2r} = \begin{cases} 1 & \text{for } r = 1, 2, \\ -1 & \text{for } r = 3, 4, \end{cases} \quad (32)$$

where $N_r(\xi^1, \xi^2)$ are the bilinear shape functions of the element; \mathbf{v}_r are the displacement vectors at element nodes; the index r runs from 1 to 4.

To implement the analytical integration throughout the element, we employ the assumed interpolation of natural strains [7, 21, 25]

$$\mathbf{E}^I = \sum_r N_r \mathbf{E}_r^I, \quad \mathbf{E}_r^I = \mathbf{E}^I(\tilde{\mathbf{P}}_r),$$

$$\mathbf{E}_r^I = [\varepsilon_{11r}^I \quad \varepsilon_{22r}^I \quad \varepsilon_{33r}^I \quad 2\varepsilon_{12r}^I \quad 2\varepsilon_{13r}^I \quad 2\varepsilon_{23r}^I]^T, \quad (33)$$

where \mathbf{E}_r^I are the strain vectors of S-surfaces at element nodes.

Remark 4

The main idea of such approach can be traced back to the ANS method [27, 28] developed by many scientists for the linear and non-linear displacement-based, hybrid and mixed isoparametric finite element formulations [1–5, 13, 16–18, 29, 30]. In contrast with above formulations, we treat the term ‘ANS’ in a broader sense. In our EG solid-shell element formulation, all components of the Green–Lagrange strain tensor are assumed to vary bilinearly inside the biunit square (Figure 5). This implies that instead of expected non-linear interpolation the more suitable bilinear ANS interpolation is used.

Remark 5

In order to circumvent curvature thickness locking for the isoparametric non-linear four-node solid-shell element, Betsch and Stein [18] proposed to apply the bilinear interpolation (33) for the transverse normal strain. It is apparent that curvature thickness locking is not related to the EG four-node solid-shell element because it can handle the arbitrary geometry of surfaces properly. We advocate the use of the modified ANS method (33) for all components of the Green–Lagrange strain tensor to implement the efficient analytical integration throughout the element.

The nodal values of strains of S-surfaces according to (A1) and (A8) are written as

$$2\varepsilon_{\alpha\beta r}^I = \frac{1}{c_{\beta r}^I} \lambda_{\alpha\beta r}^I + \frac{1}{c_{\alpha r}^I} \lambda_{\beta\alpha r}^I + \frac{1}{c_{\alpha r}^I c_{\beta r}^I} \sum_i \lambda_{i\alpha r}^I \lambda_{i\beta r}^I,$$

$$2\varepsilon_{\alpha 3r}^I = \beta_{\alpha r}^I + \frac{1}{c_{\alpha r}^I} \lambda_{3\alpha r}^I + \frac{1}{c_{\alpha r}^I} \sum_i \beta_{i\alpha r}^I \lambda_{i\alpha r}^I, \quad (34)$$

$$2\varepsilon_{33r}^I = 2\beta_{3r}^I + \sum_i \beta_{i\alpha r}^I \beta_{i\alpha r}^I,$$

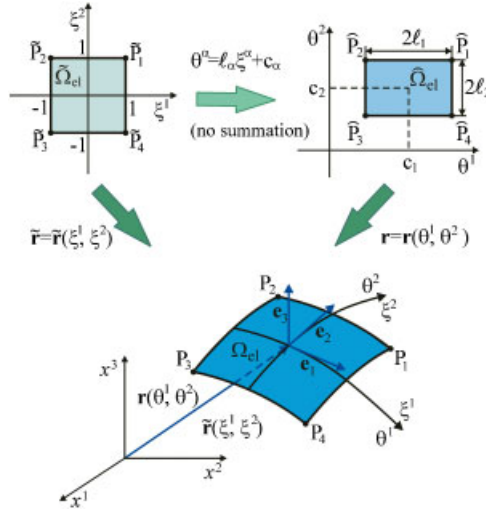


Figure 5. Biunit square in (ξ^1, ξ^2) -space mapped into the reference surface of the EG solid-shell element in (x^1, x^2, x^3) -space in the case of orthogonal coordinates θ^α .

where $c_{\alpha r}^I = 1 + k_{\alpha r} z^I$ are the nodal values of the shifter tensor at S-surfaces. Introducing further a displacement vector of the shell element

$$\mathbf{U} = [\mathbf{v}_1^T \quad \mathbf{v}_2^T \quad \mathbf{v}_3^T \quad \mathbf{v}_4^T]^T \tag{35}$$

and using (A6) and (A9), one derives the following keynote presentation for the strain parameters:

$$\lambda_{i\alpha r}^I = (\mathbf{\Lambda}_{i\alpha r}^I)^T \mathbf{U}, \quad \beta_{ir}^I = (\mathbf{\Lambda}_{i3r}^I)^T \mathbf{U}, \tag{36}$$

where $\mathbf{\Lambda}_{ijr}^I$ are the constant inside the element column matrices of order 36×1 given in Appendix B.

The use of (33), (34) and (36) yields

$$\mathbf{E}_r^I = \mathbf{B}_r^I \mathbf{U} + \mathbf{A}_r^I(\mathbf{U}) \mathbf{U}, \tag{37}$$

where \mathbf{B}_r^I and $\mathbf{A}_r^I(\mathbf{U})$ are the nodal matrices of order 6×36 corresponding to the linear and non-linear strain–displacement transformations defined as

$$\mathbf{B}_r^I = \begin{bmatrix} (c_{1r}^I)^{-1} (\mathbf{\Lambda}_{11r}^I)^T \\ (c_{2r}^I)^{-1} (\mathbf{\Lambda}_{22r}^I)^T \\ (\mathbf{\Lambda}_{33r}^I)^T \\ (c_{2r}^I)^{-1} (\mathbf{\Lambda}_{12r}^I)^T + (c_{1r}^I)^{-1} (\mathbf{\Lambda}_{21r}^I)^T \\ (\mathbf{\Lambda}_{13r}^I)^T + (c_{1r}^I)^{-1} (\mathbf{\Lambda}_{31r}^I)^T \\ (\mathbf{\Lambda}_{23r}^I)^T + (c_{2r}^I)^{-1} (\mathbf{\Lambda}_{32r}^I)^T \end{bmatrix}, \quad \mathbf{A}_r^I(\mathbf{U}) = \begin{bmatrix} \mathbf{U}^T \mathbf{\Pi}_{11r}^I \\ \mathbf{U}^T \mathbf{\Pi}_{22r}^I \\ \mathbf{U}^T \mathbf{\Pi}_{33r}^I \\ \mathbf{U}^T \mathbf{\Pi}_{12r}^I \\ \mathbf{U}^T \mathbf{\Pi}_{13r}^I \\ \mathbf{U}^T \mathbf{\Pi}_{23r}^I \end{bmatrix}, \tag{38}$$

where $\mathbf{\Pi}_{ijr}^I$ are the constant throughout the element symmetric matrices of order 36×36 given by

$$\begin{aligned} \mathbf{\Pi}_{ijr}^I &= \frac{1}{2} \sum_m \mathbf{\Lambda}_{mir}^I (\mathbf{\Lambda}_{mjr}^I)^T \quad \text{for } i = j, \\ \mathbf{\Pi}_{ijr}^I &= \frac{1}{2} \sum_m [\mathbf{\Lambda}_{mir}^I (\mathbf{\Lambda}_{mjr}^I)^T + \mathbf{\Lambda}_{mjr}^I (\mathbf{\Lambda}_{mir}^I)^T] \quad \text{for } i < j. \end{aligned} \tag{39}$$

From the computational point of view it is convenient to rewrite the ANS interpolation (33) as follows:

$$\begin{aligned}\mathbf{E}^I &= \sum_{r_1, r_2} (\xi^1)^{r_1} (\xi^2)^{r_2} \mathbf{E}^{I r_1 r_2}, \\ \mathbf{E}^{I r_1 r_2} &= \mathbf{B}^{I r_1 r_2} \mathbf{U} + \mathbf{A}^{I r_1 r_2}(\mathbf{U}) \mathbf{U}.\end{aligned}\quad (40)$$

Here and in the following developments, the indices r_1, r_2 take the values 0 and 1, and the additional notations are introduced

$$\begin{aligned}\mathbf{B}^{I00} &= \frac{1}{4}(\mathbf{B}_1^I + \mathbf{B}_2^I + \mathbf{B}_3^I + \mathbf{B}_4^I), & \mathbf{B}^{I01} &= \frac{1}{4}(\mathbf{B}_1^I + \mathbf{B}_2^I - \mathbf{B}_3^I - \mathbf{B}_4^I), \\ \mathbf{B}^{I10} &= \frac{1}{4}(\mathbf{B}_1^I - \mathbf{B}_2^I - \mathbf{B}_3^I + \mathbf{B}_4^I), & \mathbf{B}^{I11} &= \frac{1}{4}(\mathbf{B}_1^I - \mathbf{B}_2^I + \mathbf{B}_3^I - \mathbf{B}_4^I).\end{aligned}\quad (41)$$

The matrices $\mathbf{A}^{I r_1 r_2}(\mathbf{U})$ are written in a similar way by using nodal matrices $\mathbf{A}_r^I(\mathbf{U})$.

7. HYBRID STRESS–STRAIN METHOD

To improve the computational efficiency of low-order EG solid-shell elements, a hybrid method can be applied. This method is based on the robust finite element formulation pioneered by Pian [31]. In such a formulation the displacements on the element boundary are assumed to provide displacement compatibility between elements, whereas internal stresses are assumed so as to satisfy the differential equilibrium equations. The Pian's work was originally based upon the principle of the stationary complementary energy. Later, an alternative assumed stress method was proposed by applying the Hellinger–Reissner variational principle that simplifies the evaluation of the element stiffness matrix [32].

However, we do not use herein this terminology referring to Gallagher's proposal (see paper [33]), where it is said that 'the hybrid method in structural mechanics is defined at the one which is formulated by multivariable variational functional, yet the resulting matrix equations consist of only the nodal values of displacements as unknown'. Independently, the hybrid strain [10, 11, 34] and hybrid stress–strain [22] methods were developed. The former is based on the modified Hellinger–Reissner functional in which displacements and strains are utilized as fundamental shell unknowns, whereas the latter departs from the Hu–Washizu functional depending on displacements, stresses and strains.

Thus, to avoid shear and membrane locking and have no spurious zero energy modes [7, 21, 24], the assumed displacement-independent strains and stress-resultant fields throughout the element are invoked

$$\begin{aligned}\hat{\mathbf{E}}^I &= \sum_{r_1+r_2 < 2} (\xi^1)^{r_1} (\xi^2)^{r_2} \mathbf{Q}^{r_1 r_2} \hat{\mathbf{E}}^{I r_1 r_2}, \\ \hat{\mathbf{E}}^{I00} &= [\hat{\varepsilon}_{11}^{I00} \quad \hat{\varepsilon}_{22}^{I00} \quad \hat{\varepsilon}_{33}^{I00} \quad 2\hat{\varepsilon}_{12}^{I00} \quad 2\hat{\varepsilon}_{13}^{I00} \quad 2\hat{\varepsilon}_{23}^{I00}]^T, \\ \hat{\mathbf{E}}^{I01} &= [\hat{\varepsilon}_{11}^{I01} \quad \hat{\varepsilon}_{33}^{I01} \quad 2\hat{\varepsilon}_{13}^{I01}]^T, & \hat{\mathbf{E}}^{I10} &= [\hat{\varepsilon}_{22}^{I10} \quad \hat{\varepsilon}_{33}^{I10} \quad 2\hat{\varepsilon}_{23}^{I10}]^T\end{aligned}\quad (42)$$

and

$$\begin{aligned}\mathbf{H}_I &= \sum_{r_1+r_2 < 2} (\xi^1)^{r_1} (\xi^2)^{r_2} \mathbf{Q}^{r_1 r_2} \mathbf{H}_I^{r_1 r_2}, \\ \mathbf{H}_I^{00} &= [H_I^{1100} \quad H_I^{2200} \quad H_I^{3300} \quad H_I^{1200} \quad H_I^{1300} \quad H_I^{2300}]^T, \\ \mathbf{H}_I^{01} &= [H_I^{1101} \quad H_I^{3301} \quad H_I^{1301}]^T, & \mathbf{H}_I^{10} &= [H_I^{2210} \quad H_I^{3310} \quad H_I^{2310}]^T,\end{aligned}\quad (43)$$

where $\mathbf{Q}^{r_1 r_2}$ are the projective matrices defined as

$$\mathbf{Q}^{00} = \begin{bmatrix} 1 & 0 & 0 & 0 & 0 & 0 \\ 0 & 1 & 0 & 0 & 0 & 0 \\ 0 & 0 & 1 & 0 & 0 & 0 \\ 0 & 0 & 0 & 1 & 0 & 0 \\ 0 & 0 & 0 & 0 & 1 & 0 \\ 0 & 0 & 0 & 0 & 0 & 1 \end{bmatrix}, \quad \mathbf{Q}^{01} = \begin{bmatrix} 1 & 0 & 0 \\ 0 & 0 & 0 \\ 0 & 1 & 0 \\ 0 & 0 & 0 \\ 0 & 0 & 1 \\ 0 & 0 & 0 \end{bmatrix}, \quad \mathbf{Q}^{10} = \begin{bmatrix} 0 & 0 & 0 \\ 1 & 0 & 0 \\ 0 & 1 & 0 \\ 0 & 0 & 0 \\ 0 & 0 & 0 \\ 0 & 0 & 1 \end{bmatrix}. \quad (44)$$

Substituting interpolations (31), (40), (42) and (43) into the Hu-Washizu variational equation (28) and integrating analytically throughout the element, one obtains the elemental equilibrium equations of the developed finite element formulation

$$\begin{aligned} \hat{\mathbf{E}}^{I r_1 r_2} &= (\mathbf{Q}^{r_1 r_2})^T [\mathbf{B}^{I r_1 r_2} + \mathbf{A}^{I r_1 r_2}(\mathbf{U})] \mathbf{U}, \\ \mathbf{H}_I^{r_1 r_2} &= \sum_J (\mathbf{Q}^{r_1 r_2})^T \bar{\mathbf{D}}_{IJ} \mathbf{Q}^{r_1 r_2} \hat{\mathbf{E}}^{J r_1 r_2} \quad \text{for } r_1 + r_2 < 2, \\ \sum_{r_1+r_2 < 2} \sum_I \frac{1}{3^{r_1+r_2}} [\mathbf{B}^{I r_1 r_2} + 2\mathbf{A}^{I r_1 r_2}(\mathbf{U})]^T \mathbf{Q}^{r_1 r_2} \mathbf{H}_I^{r_1 r_2} &= \mathbf{F}, \end{aligned} \quad (45)$$

where \mathbf{F} is the element-wise surface traction vector. Note that a product $\sqrt{a}\Lambda$ in variational equation (28) is equal to $\ell_1 \ell_2 A_1 A_2$ (see Appendix A and Figure 5) and it is evaluated at the element center. This is because of choosing the midsurface as a reference surface and employing the orthogonal curvilinear coordinates.

8. INCREMENTAL TOTAL LAGRANGIAN FORMULATION

Up to this moment, no incremental arguments are needed in the total Lagrangian formulation. The incremental displacements, strains and stress resultants are needed for solving non-linear equations (45) on the basis of the Newton–Raphson method. Further, the left superscripts t and $t + \Delta t$ indicate in which configuration at time t or time $t + \Delta t$ a quantity occurs. Then, in accordance with this agreement we have

$$\begin{aligned} {}^{t+\Delta t} \mathbf{U} &= {}^t \mathbf{U} + \Delta \mathbf{U}, \quad {}^{t+\Delta t} \mathbf{F} = {}^t \mathbf{F} + \Delta \mathbf{F}, \\ {}^{t+\Delta t} \hat{\mathbf{E}}^{I r_1 r_2} &= {}^t \hat{\mathbf{E}}^{I r_1 r_2} + \Delta \hat{\mathbf{E}}^{I r_1 r_2}, \quad {}^{t+\Delta t} \mathbf{H}_I^{r_1 r_2} = {}^t \mathbf{H}_I^{r_1 r_2} + \Delta \mathbf{H}_I^{r_1 r_2} \quad \text{for } r_1 + r_2 < 2, \end{aligned} \quad (46)$$

where $\Delta \mathbf{U}$, $\Delta \mathbf{F}$, $\Delta \hat{\mathbf{E}}^{I r_1 r_2}$ and $\Delta \mathbf{H}_I^{r_1 r_2}$ are the incremental variables.

Substituting (46) into equilibrium equations (45) and taking into account the fact that external loads and second Piola–Kirchhoff stresses constitute the self-equilibrated system in a configuration at time t , one can obtain the incremental equations

$$\begin{aligned} \Delta \hat{\mathbf{E}}^{I r_1 r_2} &= (\mathbf{Q}^{r_1 r_2})^T [{}^t \mathbf{M}^{I r_1 r_2} + \mathbf{A}^{I r_1 r_2}(\Delta \mathbf{U})] \Delta \mathbf{U}, \\ \Delta \mathbf{H}_I^{r_1 r_2} &= \sum_J \bar{\mathbf{D}}_{IJ}^{r_1 r_2} \Delta \hat{\mathbf{E}}^{J r_1 r_2} \quad \text{for } r_1 + r_2 < 2, \end{aligned} \quad (47)$$

$$\sum_{r_1+r_2 < 2} \sum_I \frac{1}{3^{r_1+r_2}} \{ 2[\mathbf{A}^{I r_1 r_2}(\Delta \mathbf{U})]^T \mathbf{Q}^{r_1 r_2} \mathbf{H}_I^{r_1 r_2} + [{}^t \mathbf{M}^{I r_1 r_2} + 2\mathbf{A}^{I r_1 r_2}(\Delta \mathbf{U})]^T \mathbf{Q}^{r_1 r_2} \Delta \mathbf{H}_I^{r_1 r_2} \} = \Delta \mathbf{F},$$

where

$${}^t \mathbf{M}^{I r_1 r_2} = \mathbf{B}^{I r_1 r_2} + 2\mathbf{A}^{I r_1 r_2}({}^t \mathbf{U}), \quad \bar{\mathbf{D}}_{IJ}^{r_1 r_2} = (\mathbf{Q}^{r_1 r_2})^T \bar{\mathbf{D}}_{IJ} \mathbf{Q}^{r_1 r_2} \quad \text{for } r_1 + r_2 < 2. \quad (48)$$

Owing to the existence of non-linear terms in incremental equations (47), the Newton–Raphson iteration process should be employed

$$\begin{aligned}\Delta \mathbf{U}^{[k+1]} &= \Delta \mathbf{U}^{[k]} + \Delta \underline{\mathbf{U}}^{[k]}, & \Delta \hat{\mathbf{E}}^{I r_1 r_2 [k+1]} &= \Delta \hat{\mathbf{E}}^{I r_1 r_2 [k]} + \Delta \hat{\underline{\mathbf{E}}}^{I r_1 r_2 [k]}, \\ \Delta \mathbf{H}_I^{r_1 r_2 [k+1]} &= \Delta \mathbf{H}_I^{r_1 r_2 [k]} + \Delta \underline{\mathbf{H}}_I^{r_1 r_2 [k]}, & k &= 0, 1, \dots, NI,\end{aligned}\quad (49)$$

where NI is the number of iterations. As a result, the linearized equilibrium equations are expressed as

$$\begin{aligned}\Delta \hat{\underline{\mathbf{E}}}^{I r_1 r_2 [k]} - (\mathbf{Q}^{r_1 r_2})^T {}^t \mathbf{L}^{I r_1 r_2 [k]} \Delta \underline{\mathbf{U}}^{[k]} &= (\mathbf{Q}^{r_1 r_2})^T [{}^t \mathbf{L}^{I r_1 r_2 [k]} - \mathbf{A}^{I r_1 r_2}(\Delta \mathbf{U}^{[k]})] \Delta \mathbf{U}^{[k]} - \Delta \hat{\mathbf{E}}^{I r_1 r_2 [k]}, \\ \Delta \underline{\mathbf{H}}_I^{r_1 r_2 [k]} - \sum_J \bar{\mathbf{D}}_{IJ}^{r_1 r_2} \Delta \hat{\underline{\mathbf{E}}}^{J r_1 r_2 [k]} &= 0 \quad \text{for } r_1 + r_2 < 2, \\ \sum_{r_1+r_2 < 2} \sum_I \frac{1}{3^{r_1+r_2}} \{2[\mathbf{A}^{I r_1 r_2}(\Delta \underline{\mathbf{U}}^{[k]})]^T \mathbf{Q}^{r_1 r_2} ({}^t \mathbf{H}_I^{r_1 r_2} + \Delta \mathbf{H}_I^{r_1 r_2 [k]}) &+ ({}^t \mathbf{L}^{I r_1 r_2 [k]})^T \mathbf{Q}^{r_1 r_2} \Delta \underline{\mathbf{H}}_I^{r_1 r_2 [k]}\} \\ &= \Delta \mathbf{F} - \sum_{r_1+r_2 < 2} \sum_I \frac{1}{3^{r_1+r_2}} \{2[\mathbf{A}^{I r_1 r_2}(\Delta \mathbf{U}^{[k]})]^T \mathbf{Q}^{r_1 r_2} {}^t \mathbf{H}_I^{r_1 r_2} &+ ({}^t \mathbf{L}^{I r_1 r_2 [k]})^T \mathbf{Q}^{r_1 r_2} \Delta \mathbf{H}_I^{r_1 r_2 [k]}\},\end{aligned}\quad (50)$$

where

$${}^t \mathbf{L}^{I r_1 r_2 [k]} = \mathbf{B}^{I r_1 r_2} + 2\mathbf{A}^{I r_1 r_2} ({}^t \mathbf{U} + \Delta \mathbf{U}^{[k]}) \quad \text{for } r_1 + r_2 < 2. \quad (51)$$

Eliminating incremental displacement-independent strains $\Delta \hat{\underline{\mathbf{E}}}^{I r_1 r_2 [k]}$ and stress resultants $\Delta \underline{\mathbf{H}}_I^{r_1 r_2 [k]}$ from (50) and introducing symmetric matrices

$$\mathbf{D}_{IJ}^{r_1 r_2} = \mathbf{Q}^{r_1 r_2} \bar{\mathbf{D}}_{IJ}^{r_1 r_2} (\mathbf{Q}^{r_1 r_2})^T = \mathbf{Q}^{r_1 r_2} (\mathbf{Q}^{r_1 r_2})^T \mathbf{D}_{IJ} \mathbf{Q}^{r_1 r_2} (\mathbf{Q}^{r_1 r_2})^T \quad \text{for } r_1 + r_2 < 2, \quad (52)$$

$$\mathbf{R}^{I r_1 r_2}(\mathbf{H}_I) = \sum_{i \leq j} H_I^{ij} \Pi_{ij}^{I r_1 r_2} \quad \text{for } r_1 + r_2 < 2, \quad (53)$$

$$\begin{aligned}\Pi_{ij}^{I 00} &= \frac{1}{4}(\Pi_{ij1}^I + \Pi_{ij2}^I + \Pi_{ij3}^I + \Pi_{ij4}^I), & \Pi_{ij}^{I 01} &= \frac{1}{4}(\Pi_{ij1}^I + \Pi_{ij2}^I - \Pi_{ij3}^I - \Pi_{ij4}^I), \\ \Pi_{ij}^{I 10} &= \frac{1}{4}(\Pi_{ij1}^I - \Pi_{ij2}^I - \Pi_{ij3}^I + \Pi_{ij4}^I)\end{aligned}\quad (54)$$

one derives a system of linearized element equations

$$\mathbf{K}_T \Delta \underline{\mathbf{U}}^{[k]} = \Delta \mathbf{F}^{[k]}, \quad (55)$$

where $\mathbf{K}_T = \mathbf{K}_D + \mathbf{K}_H$ is the tangent stiffness matrix; $\Delta \mathbf{F}^{[k]}$ is the right-hand side vector given by

$$\mathbf{K}_D = \sum_{r_1+r_2 < 2} \frac{1}{3^{r_1+r_2}} \sum_{I,J} ({}^t \mathbf{L}^{I r_1 r_2 [k]})^T \mathbf{D}_{IJ}^{r_1 r_2} {}^t \mathbf{L}^{J r_1 r_2 [k]}, \quad (56)$$

$$\mathbf{K}_H = 2 \sum_{r_1+r_2 < 2} \frac{1}{3^{r_1+r_2}} \sum_I \mathbf{R}^{I r_1 r_2} [\mathbf{Q}^{r_1 r_2} ({}^t \mathbf{H}_I^{r_1 r_2} + \Delta \mathbf{H}_I^{r_1 r_2 [k]})], \quad (57)$$

$$\begin{aligned}\Delta \mathbf{F}^{[k]} &= \Delta \mathbf{F} - \sum_{r_1+r_2 < 2} \frac{1}{3^{r_1+r_2}} \left\{ \sum_{I,J} ({}^t \mathbf{L}^{I r_1 r_2 [k]})^T \mathbf{D}_{IJ}^{r_1 r_2} [{}^t \mathbf{L}^{J r_1 r_2 [k]} - \mathbf{A}^{J r_1 r_2}(\Delta \mathbf{U}^{[k]})] \right. \\ &\quad \left. + 2 \sum_I \mathbf{R}^{I r_1 r_2} (\mathbf{Q}^{r_1 r_2} {}^t \mathbf{H}_I^{r_1 r_2}) \right\} \Delta \mathbf{U}^{[k]}.\end{aligned}\quad (58)$$

To find the tangent stiffness matrix, the useful matrix transformation

$$[\mathbf{A}^{I r_1 r_2}(\mathbf{U})]^T \mathbf{H}_I = \mathbf{R}^{I r_1 r_2}(\mathbf{H}_I) \mathbf{U} \quad \text{for } r_1 + r_2 < 2 \quad (59)$$

should be invoked.

As expected, the tangent stiffness matrix is symmetric. This is due to the fact that both matrices \mathbf{K}_D and \mathbf{K}_H are symmetric. The proof of symmetry of the latter matrix follows from notations (29), (39), (53) and (54).

Remark 6

For computing the mode stress-resultant vectors from (57), we employ the advanced finite element technique, that is

$$\Delta \mathbf{H}_I^{r_1 r_2 [k]} = \sum_J \bar{\mathbf{D}}_{IJ}^{r_1 r_2} \Delta \hat{\mathbf{E}}^{J r_1 r_2 [k]} \quad \text{for } r_1 + r_2 < 2, \quad (60)$$

$$\begin{aligned} \Delta \hat{\mathbf{E}}^{J r_1 r_2 [k]} = & (\mathbf{Q}^{r_1 r_2})^T [{}^t \mathbf{M}^{J r_1 r_2} \Delta \mathbf{U}^{[k]} + 2 \mathbf{A}^{J r_1 r_2} (\Delta \mathbf{U}^{[k-1]}) \Delta \underline{\mathbf{U}}^{[k-1]} \\ & + \mathbf{A}^{J r_1 r_2} (\Delta \mathbf{U}^{[k-1]}) \Delta \mathbf{U}^{[k-1]}] \quad \text{for } r_1 + r_2 < 2, \end{aligned} \quad (61)$$

where $\Delta \underline{\mathbf{U}}^{[k-1]} = \Delta \mathbf{U}^{[k]} - \Delta \mathbf{U}^{[k-1]}$. These formulas hold for $k \geq 1$, whereas at the beginning of each iteration process one has to set

$$\Delta \mathbf{U}^{[0]} = \mathbf{0} \quad \text{and} \quad \Delta \hat{\mathbf{E}}^{J r_1 r_2 [0]} = \mathbf{0}.$$

The proposed incremental approach allows the use of load increments, which are much larger than possible with standard displacement-based EG shell element formulations [6, 12]. This is because of the fact that an additional load vector due to compatibility mismatch (61) at the k th iteration step is present in linearized equilibrium equations (55) and disappears only at the end of the iteration process as discussed, e.g. in [11, 21, 25, 35, 36].

Remark 7

It is necessary to note that the elemental matrices (56)–(58) require only direct substitutions, i.e. no expensive matrix inversion is needed to derive them. This is unusual for the isoparametric hybrid/mixed finite element formulations [10, 11, 13, 16]. Furthermore, all element matrices are evaluated by using analytical integration throughout the element. Thus, our EG solid-shell element formulation is economical and efficient compared to the conventional isoparametric solid-shell element formulations because it additionally permits the use of coarser mesh configurations.

Remark 8

It is of extreme interest to notice that the nodal displacement vectors $\mathbf{u}_r^2 = [u_{1r}^2 \ u_{2r}^2 \ u_{3r}^2 \ u_{4r}^2]^T$ corresponding to the inner S-surface can be statically condensed out at the element level to reduce the number of degrees of freedom to 24. Therefore, such an approach does not introduce any additional degrees of freedom at the global level and is very similar to the 6-parameter solid-shell element formulation [10–18]. However, the reduced number of degrees of freedom restricts the possibility of studying some 3D problems for thick shells with specific boundary conditions at the shell edges as discussed in Section 9.5. Thus, we do not utilize such a technology at this stage of our finite element developments.

The equilibrium equations (55) for each element are assembled by the usual technique to form the global equilibrium equations. These equations have to be performed until the required accuracy of the solution can be obtained. To realize the above, the displacement-based convergence criterion is employed

$$\|\mathbf{U}_G^{[k+1]} - \mathbf{U}_G^{[k]}\| < \varepsilon \|\mathbf{U}_G^{[k]}\|, \quad (62)$$

where $\|\bullet\|$ denotes the Euclidean norm; \mathbf{U}_G is the global displacement vector; ε is the prescribed tolerance.

9. GEOMETRICALLY LINEAR ANALYSIS

9.1. On the selection of displacement-independent strain field

The assumed strain field (42) is selected such that the 12-node finite element developed will be free of locking and kinematically stable. To circumvent a locking phenomenon, the assumed strain field should be chosen to be as simple as possible. One can suppose that the simplest element approximation for the transverse normal strain

$$\hat{\varepsilon}_{33}^I = \hat{\varepsilon}_{33}^{I00} \quad (63)$$

is sufficient for this purpose. However, the use of 10 assumed strain parameters for each S-surface yields two spurious kinematic modes. This fact is addressed below. Much better results one can achieve employing a linear interpolation for the transverse normal strain (42), that is

$$\hat{\varepsilon}_{33}^I = \hat{\varepsilon}_{33}^{I00} + \xi^1 \hat{\varepsilon}_{33}^{I10} + \xi^2 \hat{\varepsilon}_{33}^{I01}. \quad (64)$$

As a result, 12 assumed strain parameters are introduced for each S-surface. It seems to be excessive recalling about three displacement degrees of freedom per node. Fortunately, there exist six dependent strain modes exactly, which provide a correct rank of the element matrix.

These dependent modes can be determined analytically in the case of flat element geometry and expressed as

$$\begin{aligned} \hat{\varepsilon}_{33}^{100} - 2\hat{\varepsilon}_{33}^{200} + \hat{\varepsilon}_{33}^{300} &= 0, & \hat{\varepsilon}_{33}^{110} - 2\hat{\varepsilon}_{33}^{210} + \hat{\varepsilon}_{33}^{310} &= 0, & \hat{\varepsilon}_{33}^{101} - 2\hat{\varepsilon}_{33}^{201} + \hat{\varepsilon}_{33}^{301} &= 0, \\ \hat{\varepsilon}_{13}^{101} - 2\hat{\varepsilon}_{13}^{201} + \hat{\varepsilon}_{13}^{301} &= \hat{\varepsilon}_{23}^{110} - 2\hat{\varepsilon}_{23}^{210} + \hat{\varepsilon}_{23}^{310}, \\ \hat{\varepsilon}_{13}^{100} - 2\hat{\varepsilon}_{13}^{200} + \hat{\varepsilon}_{13}^{300} &= \frac{1}{8}h(-\hat{\varepsilon}_{33}^{110} + \hat{\varepsilon}_{33}^{310}), & \hat{\varepsilon}_{23}^{100} - 2\hat{\varepsilon}_{23}^{200} + \hat{\varepsilon}_{23}^{300} &= \frac{1}{8}h(-\hat{\varepsilon}_{33}^{101} + \hat{\varepsilon}_{33}^{301}). \end{aligned} \quad (65)$$

Indeed, the use of the bilinear interpolation for the displacement field

$$u_i^I = u_i^{I00} + \xi^1 u_i^{I10} + \xi^2 u_i^{I01} + \xi^1 \xi^2 u_i^{I11} \quad (66)$$

and strain–displacement relationships (A6), (A8) and (A9), which can be written for the transverse strain components as

$$\begin{aligned} 2\varepsilon_{13}^{I00} &= u_3^{I10} + \beta_1^{I00}, & 2\varepsilon_{13}^{I01} &= u_3^{I11} + \beta_1^{I01}, \\ 2\varepsilon_{23}^{I00} &= u_3^{I01} + \beta_2^{I00}, & 2\varepsilon_{23}^{I10} &= u_3^{I11} + \beta_2^{I10}, \\ \varepsilon_{33}^{I r_1 r_2} &= \beta_3^{I r_1 r_2}, & \beta_i^{I r_1 r_2} &= \frac{1}{h}(-3u_i^{1 r_1 r_2} + 4u_i^{2 r_1 r_2} - u_i^{3 r_1 r_2}), \\ \beta_i^{2 r_1 r_2} &= \frac{1}{h}(-u_i^{1 r_1 r_2} + u_i^{3 r_1 r_2}), & \beta_i^{3 r_1 r_2} &= \frac{1}{h}(u_i^{1 r_1 r_2} - 4u_i^{2 r_1 r_2} + 3u_i^{3 r_1 r_2}) \quad \text{for } r_1 + r_2 < 2 \end{aligned} \quad (67)$$

leads to the following coupling equations:

$$\begin{aligned} \varepsilon_{33}^{100} - 2\varepsilon_{33}^{200} + \varepsilon_{33}^{300} &= 0, & \varepsilon_{33}^{110} - 2\varepsilon_{33}^{210} + \varepsilon_{33}^{310} &= 0, & \varepsilon_{33}^{101} - 2\varepsilon_{33}^{201} + \varepsilon_{33}^{301} &= 0, \\ \varepsilon_{13}^{101} - 2\varepsilon_{13}^{201} + \varepsilon_{13}^{301} &= \varepsilon_{23}^{110} - 2\varepsilon_{23}^{210} + \varepsilon_{23}^{310}, \\ \varepsilon_{13}^{100} - 2\varepsilon_{13}^{200} + \varepsilon_{13}^{300} &= \frac{1}{8}h(-\varepsilon_{33}^{110} + \varepsilon_{33}^{310}), & \varepsilon_{23}^{100} - 2\varepsilon_{23}^{200} + \varepsilon_{23}^{300} &= \frac{1}{8}h(-\varepsilon_{33}^{101} + \varepsilon_{33}^{301}). \end{aligned} \quad (68)$$

Recalling the element equations (40) and (45) for the transverse strain components

$$\begin{aligned} \hat{\varepsilon}_{i3}^{I00} &= \varepsilon_{i3}^{I00}, & \hat{\varepsilon}_{13}^{I01} &= \varepsilon_{13}^{I01}, & \hat{\varepsilon}_{23}^{I10} &= \varepsilon_{23}^{I10}, \\ \hat{\varepsilon}_{33}^{I01} &= \varepsilon_{33}^{I01}, & \hat{\varepsilon}_{33}^{I10} &= \varepsilon_{33}^{I10} \end{aligned} \quad (69)$$

one can observe that coupling equations (65) and (68) are equivalent.

Coupling equations (65) play a central role in the proposed hybrid stress–strain finite element formulation because they imply that only 30 assumed strain modes are independent of 36 ones

introduced by (42). Therefore, the element stiffness matrix has six, and only six, zero eigenvalues as required for satisfaction of the general rigid-body motion representation. Unfortunately, last three coupling equations (65) can be fulfilled only approximately for the general shell geometry. Such a defect reduces the accuracy of calculating the eigenvalues corresponding to rotational rigid-body modes but has no effect on the performance of the EG 12-node solid-shell element developed.

9.2. Square plate supported at four corners

A square plate supported at four corners and subjected to uniform pressure is considered to assess the ability of the proposed EG solid-shell element EG9P4 to model rigid-body motions. The geometrical and material characteristics of the plate are presented in Figure 6.

Owing to symmetry of the problem, only one quarter of the plate is discretized by regular meshes of EG9P4 elements. Figure 7 shows the variation of the transverse midplane displacement u_3^2 along the centerline AB employing 8×8 meshes at each S-surface and a comparison with Reissner–Mindlin plate elements [37, 38]. Table I lists the results of the convergence study due to mesh refinement by using a transverse displacement at the central point $u_3^2(0, 0)$ compared with the plate element [39] in which the Kirchhoff constraints are fulfilled at discrete points. One can see that the EG9P4 element represents rigid-body plate motions properly and it is free from locking.

In order to get more information concerning zero energy modes, the eigenvalues for a single EG9P4 element are listed in Table II. It is seen that six zero energy modes are observed. All other

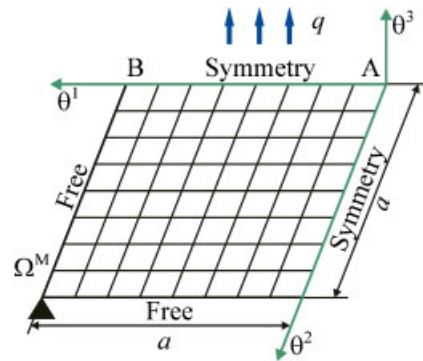


Figure 6. Square plate supported at four corners with $a = 12$, $h = 0.375$, $E = 4.3 \times 10^5$, $\nu = 0.38$ and $q = 0.03125$.

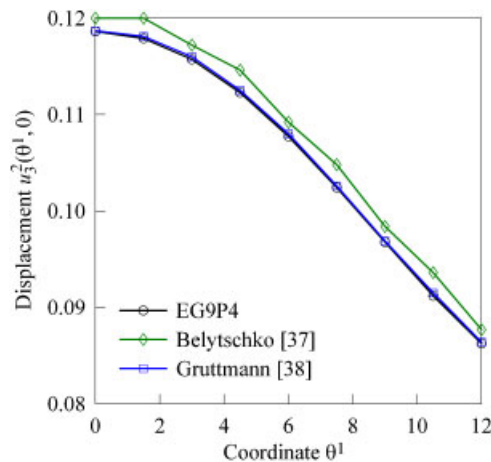


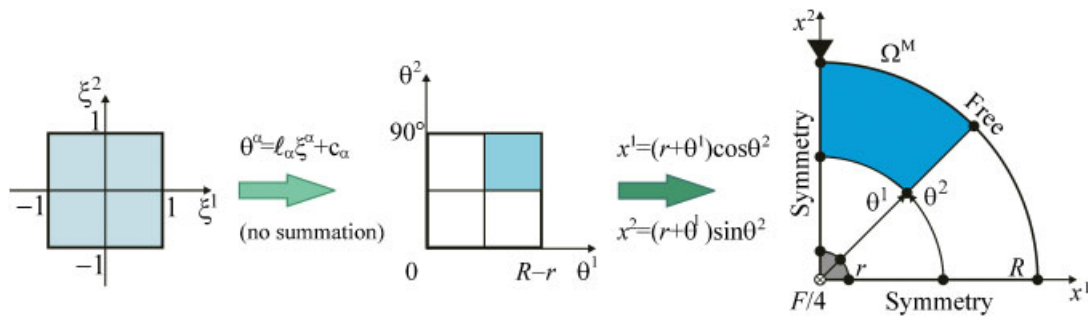
Figure 7. Variation of the transverse displacement along the centerline.

Table I. Convergence results for a square plate using a transverse displacement $u_3^2(0, 0)$.

Element	8×8	16×16	24×24	48×48	96×96
Batoz [39]	0.11914	0.11960	0.11969	0.11974	0.11975
EG9P4	0.11863	0.11998	0.12048	0.12083	0.12107

Table II. Eigenvalues for the square plate supported at four corners (Plate 1), circular plate supported at two points (Plate 2), spherical shell under inner pressure (Shell 1), pinched cylindrical shell (Shell 2) and cylindrical shell under end stretching (Shell 3).

Number	1	2	3	4	5	6	7	...	36
Plate 1	4.66E-10	1.02E-9	4.04E-9	1.35E-8	1.40E-8	4.24E-8	2.53E+0	...	6.18E+8
Plate 2	7.99E-10	4.21E-9	5.49E-9	3.53E-6	5.29E-6	6.74E-6	1.30E+2	...	2.28E+11
Shell 1	8.69E-10	3.35E-9	4.41E-9	8.53E-7	1.18E-6	2.37E-6	1.57E+1	...	9.23E+10
Shell 2	3.78E-7	9.79E-7	4.90E-6	5.88E-6	8.99E-6	1.53E-5	9.94E+0	...	3.81E+11
Shell 3	2.29E-9	3.10E-8	5.49E-8	7.85E-8	1.17E-7	3.19E-7	2.02E+4	...	3.39E+9

Figure 8. Circular plate supported at two points with $R=10$, $r=0.001$, $h=0.1$, $E=10^5$, $\nu=0.25$ and $F=1$.

deformation modes are associated with nonzero eigenvalues. It should be mentioned that computations were performed on a standard PC employing the 16-digit calculation.

9.3. Circular plate supported at two points

Consider a circular plate of the radius R with a small rigid circular inclusion of the radius r at its center. The plate is supported at two diametrically opposite points and subjected to a concentrated load F at its center. Such a problem is an excellent test to verify again the ability of the EG9P4 element to model rigid-body motions and assess the analytical integration schemes developed. This is because of the fact that we utilize just elemental nodes to evaluate the stiffness matrix, i.e. no Gauss sampling points are employed and we deal here with a shell of revolution with geometrical parameters

$$A_1 = 1, \quad A_2 = r + \theta^1, \quad k_1 = k_2 = 0, \quad \theta^1 \in [0, R - r]. \quad (70)$$

Owing to symmetry of the problem, only one quarter of the plate is discretized by uniform meshes shown in Figure 8. Table III lists results of the convergence study through using two values of the transverse displacement $u_3^2(0, 0)$ and $u_3^2(R - r, 0)$ compared with the analytical solution [40] of the Kirchhoff plate theory (CPT). Additionally, we represent in Table II the eigenvalues for a single EG9P4 element. It is seen that in this specific shell problem there exist six zero energy modes as in a previous flat shell example but the accuracy of calculating the eigenvalues corresponding to rotational rigid-body modes is worse; see on this subject Section 9.1.

Table III. Convergence results for a circular plate using the transverse midsurface displacement $\tilde{u}_3^2 = Du_3^2 / FR^2$.

Mesh	2 × 2	4 × 4	8 × 8	16 × 16	32 × 32	CPT [40]
$\tilde{u}_3^2(0, 0)$	0.0999	0.1136	0.1162	0.1167	0.1168	0.116
$\tilde{u}_3^2(R - r, 0)$	0.0931	0.1117	0.1164	0.1177	0.1180	0.118

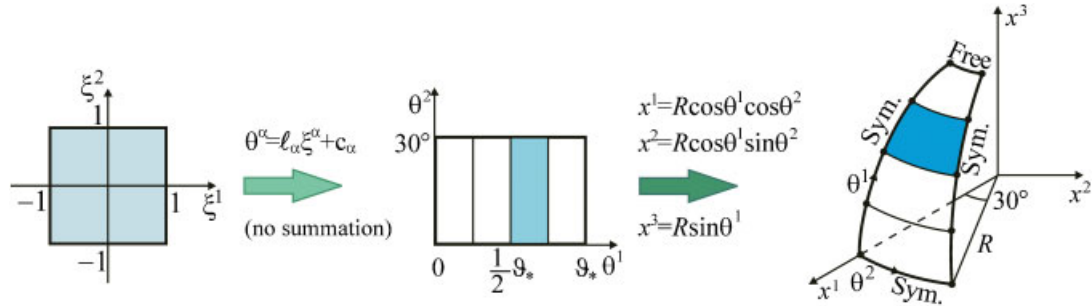


Figure 9. Spherical shell with $R = 10$, $h = 0.1$, $\vartheta_* = 89.98^\circ$, $E = 10^5$, $\nu = 0.3$ and $q = 1$.

Table IV. Convergence results for a spherical shell using the transverse displacement $\tilde{u}_3 = 10^3 u_3^3(0, 0)$ and normal strains $\tilde{\varepsilon}_{ii} = 10^4 \varepsilon_{ii}^3(0, 0)$ at the outer surface.

Mesh	2 × 1	4 × 1	8 × 1	16 × 1	32 × 1	64 × 1	Elasticity [41]
\tilde{u}_3	3.750	3.533	3.482	3.469	3.466	3.465	3.465
$\tilde{\varepsilon}_{11}$	3.805	3.515	3.464	3.452	3.449	3.448	3.448
$\tilde{\varepsilon}_{22}$	3.804	3.515	3.464	3.452	3.449	3.448	3.448
$-\tilde{\varepsilon}_{33}$	3.341	3.012	2.969	2.958	2.956	2.955	2.955

9.4. Spherical shell under inner pressure

Next, we consider a spherical shell with 0.02° hole at the top subjected to inner pressure q . This problem is also a good benchmark to test the proposed analytical integration technique and confirm that the finite element formulation developed is able to reproduce constant stress–strain states. To compare the results derived, we invoke Lamé’s solution [41], which can be written as

$$u_r = \frac{qa^3}{E(b^3 - a^3)} \left[(1 - 2\nu)r + (1 + \nu)\frac{b^3}{2r^2} \right], \quad \varepsilon_r = \frac{du_r}{dr}, \tag{71}$$

$$\varepsilon_\theta = \varepsilon_\varphi = \frac{u_r}{r}, \quad a = R - \frac{1}{2}h, \quad b = R + \frac{1}{2}h,$$

where r is the radial distance from a point to the origin; R is the radius of the midsurface.

Owing to symmetry, we consider a part of the shell, which is modeled by regular meshes depicted in Figure 9. Table IV and Figure 10 display the results of the convergence study due to mesh refinement. As can be seen, the EG9P4 element passes a constant strain test even for coarse meshes. Table II lists the eigenvalues for a single EG9P4 element. One can observe that there are again six zero energy modes exactly as in a previous shell example but the accuracy of computations is slightly better.

9.5. Pinched cylindrical shell

To illustrate the capability of the proposed solid-shell element EG9P4 to overcome shear and membrane locking and to compare it with high performance isoparametric four-node shell elements

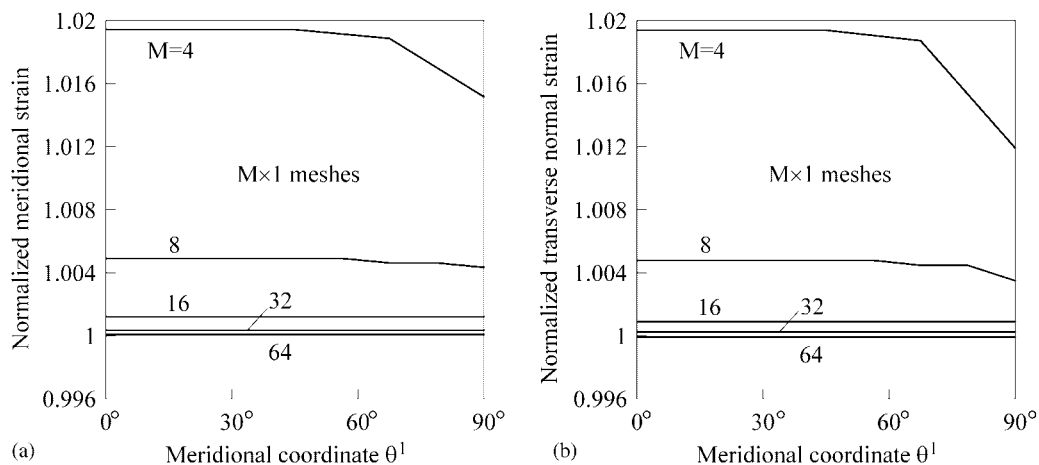


Figure 10. Variation of normalized strains at the inner surface along a meridian $\theta^2=0$: (a) meridional strain $(\epsilon_{11}^1)^{Norm}$ and (b) transverse normal strain $(\epsilon_{33}^1)^{Norm}$.

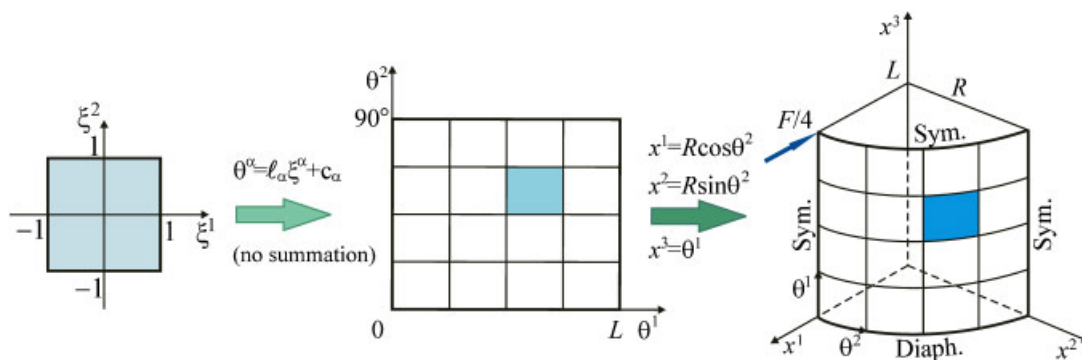


Figure 11. Pinched cylindrical shell with $R=300$, $L=300$, $h=3$, $E=3 \times 10^6$, $\nu=0.3$ and $F=1$.

Table V. Normalized transverse displacement at the load point.

Mesh	EG shell elements				Isoparametric shell elements			
	EG9P4	EG7P4 [7]	EG6P4 [15]	EG5P4 [46]	Bathe [29]	Hughes [42]	Liu [43]	Simo [44]
4 × 4	0.8520	0.8448	0.8900	0.8875	0.370	0.373	0.469	0.399
8 × 8	0.9166	0.9121	0.9412	0.9390	0.740	0.747	0.791	0.763
16 × 16	0.9746	0.9720	0.9861	0.9836	0.930	0.935	0.946	0.935

[29, 42–44], we consider one of the most demanding standard tests in which shear locking is much greater than membrane locking [45]. A short cylindrical shell supported by two rigid diaphragms at the ends is loaded by two opposite concentrated loads in its middle section as depicted in Figure 11.

Owing to symmetry of the problem, only one octant of the shell is modeled with regular meshes. Table V lists the normalized transverse displacement under the applied load and a comparison with aforementioned 5-parameter isoparametric four-node shell elements and 5-, 6- and 7-parameter EG four-node shell elements [7, 15, 46]. The displacements are normalized with respect to the analytical solution -1.8248×10^{-5} [47] based on the Kirchhoff–Love shell theory. It is seen that all EG shell elements exhibit an excellent performance even for coarse mesh configurations. The eigenvalues of the single EG9P4 element are listed in Table II.

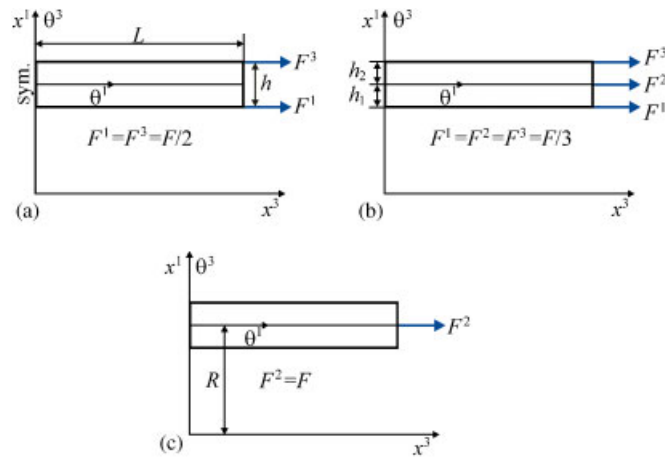


Figure 12. Two-layer cylindrical shell with $R=100$, $L=50$, $h_1=h_2=10$, $E_L=25E_T$, $E_T=10^6$, $G_{LT}=0.5E_T$, $G_{TT}=0.2E_T$, $\nu_{LT}=\nu_{TT}=0.25$: (a) loading condition A; (b) loading condition B; and (c) loading condition C.

9.6. Cylindrical shell under end stretching

To evaluate the transverse normal deformation response, we consider a thick two-layer cylindrical shell under end stretching [48]. The material and geometrical characteristics of the shell are presented in Figure 12 and a ply sequence is taken to be $[30/-30]$. A shell is subjected to axial line loads F^l , which are distributed along the circles belonging S-surfaces such that the resulting load equals F precisely. To investigate this problem more carefully, we consider three types of loading, namely

$$F^1 = F^3 = F/2, \quad (72A)$$

$$F^1 = F^2 = F^3 = F/3, \quad (72B)$$

$$F^2 = F. \quad (72C)$$

It should be noticed that only first type of loading (72A) could be realized within the framework of 6- and 7-parameter shell descriptions.

Owing to symmetry of the problem, only half of the shell is modeled with 32 axisymmetric EG9P4 elements. Figure 13 shows displacements of the bottom and top surfaces \bar{u}_i^1 and \bar{u}_i^3 for all types of loading, where $\bar{u}_i^l = 10E_T R u_i^l / F$. It is interesting to note that a shell behavior is unusual to the region $0 \leq \theta^1 < 40$ for loading conditions (72A) and (72B) since the thickness change $\Delta h = u_3^3 - u_3^1$ is positive. This means that a shell thickness increases. On the contrary, the use of loading condition (72C) leads to increasing the shell thickness in the end region $40 < \theta^1 \leq 50$.

10. GEOMETRICALLY NON-LINEAR ANALYSIS

The performance of the proposed EG 12-node solid-shell element EG9P4 is evaluated by compared with non-linear isoparametric shell elements extracted from the literature. All our results are compared with those based on using identical node spacing, the same convergence criterion (62) and tolerance $\varepsilon = 10^{-4}$. In each numerical example, N_{Step} denotes the number of load steps employed to *equally* divide the maximum load, whereas N_{Iter} stands for the total number of iterations.

10.1. Slit ring plate under line load

This example is considered in the literature to test non-linear finite element formulations for thin-walled shell structures and has been extensively used by many investigators. The ring plate is

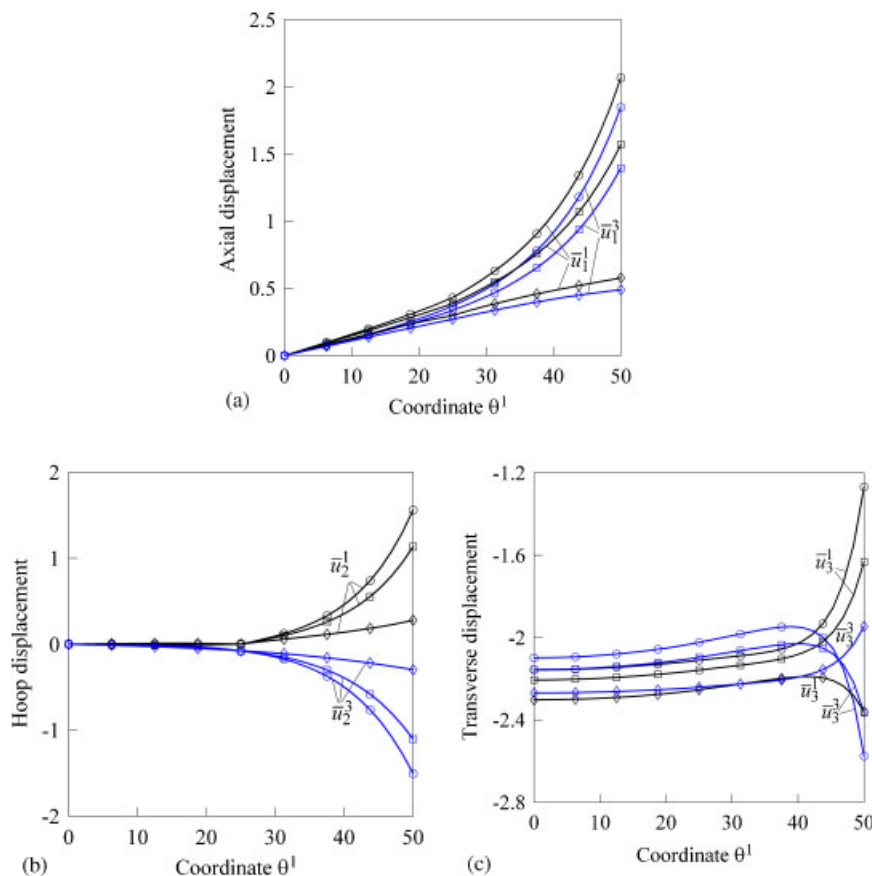


Figure 13. Displacements of external surfaces of the angle-ply cylindrical shell: (a) axial \bar{u}_1^I , (b) circumferential \bar{u}_2^I and (c) transverse \bar{u}_3^I ; results on the bases of loading conditions (72A), (72B) and (72C) are represented through curves marked by \circ , \square and \diamond .

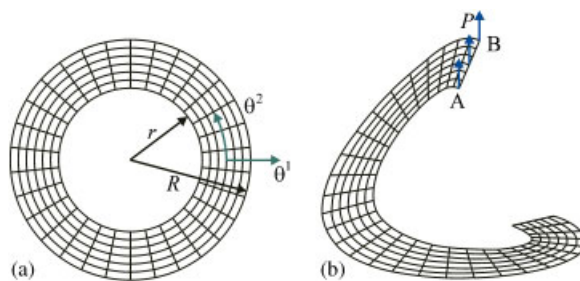


Figure 14. Slit ring plate with $r=6$, $R=10$, $h=0.03$, $E=2.1 \times 10^7$, $\nu=0$ and $P=0.8$: (a) geometry and (b) deformed configuration (modeled by 6×30 mesh).

subjected to a line load P applied at its free edge of the slit, whereas the other edge is fully clamped (Figure 14).

The displacements at points A and B of the plate, presented in Table VI and Figure 15, have been found by employing uniform meshes of EG9P4 elements. A comparison with EG four-node solid-shell elements [7] and ABAQUS S4R element [49] is also given. As can be seen, extremely coarse mesh configurations with the EG9P4 element can be used because the 2×4 mesh already yields 91% of the reference solution provided by the S4R element. Note also that in this case only six Newton iterations are needed to find a converged solution with the chosen criterion and tolerance.

Table VI. Midplane displacements at points A and B of the slit ring plate using criterion (62) with tolerance of 10^{-4} .

Element Mesh	EG9P4 2×4	EG9P4 4×8	EG9P4 16×32	EG9P4 10×80	EG7P4 [7] 10×80	EG6P4 [7] 10×80	S4R [49] 10×80
$u_3(A)$	12.739	12.574	13.670	13.760	13.765	13.760	13.891
$u_3(B)$	16.025	16.092	17.302	17.398	17.402	17.398	17.528
N_{Step}/N_{Iter}	1/6	1/8	1/10	1/11	1/13	1/12	640/346 ^a

^a $N_{Iter} = 346$ in the case of using 67 non-uniform load increments [49].

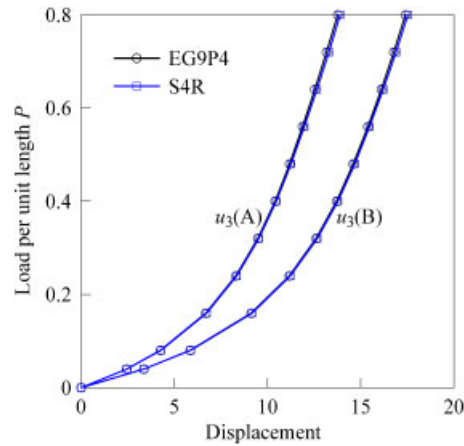
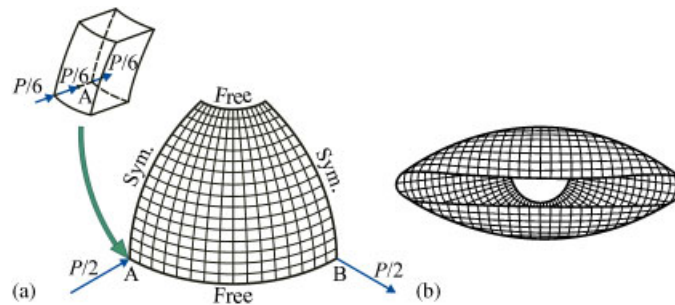
Figure 15. Midplane displacements of the slit ring plate (modeled by 10×80 mesh).

Figure 16. Pinched hemispherical shell with $R=10$, $h=0.04$, hole= 18° , $E=6.825 \times 10^7$, $\nu=0.3$, $P=100f$ and $f=4$: (a) geometry and (b) deformed configuration (modeled by 16×16 mesh).

10.2. Pinched hemispherical shell

To investigate the capability of the proposed EG solid-shell element EG9P4 to model the inextensional bending and large rigid-body motions, we consider one of the most demanding non-linear tests. A hemispherical shell with 18° hole at the top is loaded by two pairs of opposite forces on the equator. The geometrical and material data of the problem are shown in Figure 16.

Owing to symmetry, only one quarter of the shell is modeled with regular meshes of EG9P4 elements. Table VII lists midsurface displacements under applied loads employing EG solid-shell elements and ABAQUS S4R element [49]. One can observe that the EG9P4 element is a bit stiff compared with the EG6P4 element because of utilizing the complete 3D constitutive equations. At the same time it performs excellently for coarse meshes. For example, a very coarse mesh 4×4 yields 86% of the reference displacement value at point A provided by the S4R element. Figure 17 displays load–displacement curves compared with those derived by the 16×16 mesh of S4R shell elements. It is seen that the results agree closely.

Table VII. Midsurface displacements at points A and B of the pinched hemispherical shell using criterion (62) with tolerance of 10^{-4} .

Element Mesh	EG9P4 4 × 4	EG9P4 8 × 8	EG9P4 16 × 16	EG7P4 [7] 16 × 16	EG6P4 [7] 16 × 16	S4R [49] 16 × 16
$u_3(B)$	3.2609	3.9526	4.0509	4.0545	4.0557	4.067
$-u_3(A)$	7.0549	8.1047	8.1322	8.1232	8.1451	8.178
N_{Step}/N_{Iter}	1/7	1/7	1/7	1/7	1/7	40/136 ^a

^a $N_{Iter} = 136$ in the case of using 27 non-uniform load increments [49].

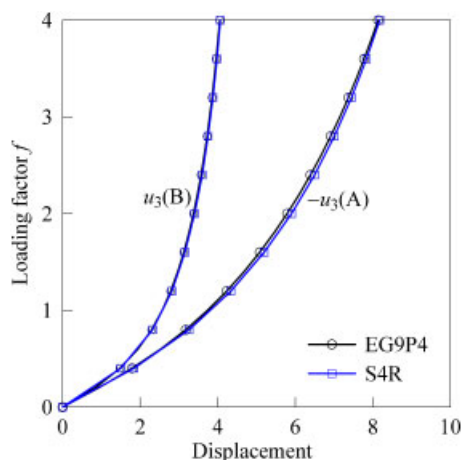
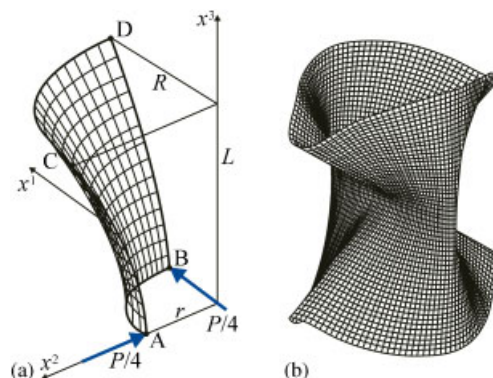
Figure 17. Midsurface displacements of the pinched hemispherical shell (modeled by 16×16 mesh).

Figure 18. Pinched three-layer hyperbolic shell with $r=7.5$, $R=15$, $L=20$, $h=0.04$, $h_0=h/3$, $E_L=4 \times 10^7$, $E_T=10^6$, $G_{LT}=G_{TT}=6 \times 10^5$, $\nu_{LT}=\nu_{TT}=0.25$, $P=80f$ and $f=5$: (a) geometry and (b) deformed configuration for the $[90/0/90]$ ply orientation.

10.3. Pinched three-layer hyperbolic shell

Further, we consider cross-ply hyperbolic shells under two pairs of opposite forces. The geometrical and material data of the three-layer hyperbolic shell are shown in Figure 18. Two cross-ply hyperbolic shells with different ply orientations $[0/90/0]$ and $[90/0/90]$ but the same ply thickness $[h_0/h_0/h_0]$ are investigated, where 0 and 90° are referred to the circumferential and meridional directions as accepted in this benchmark.

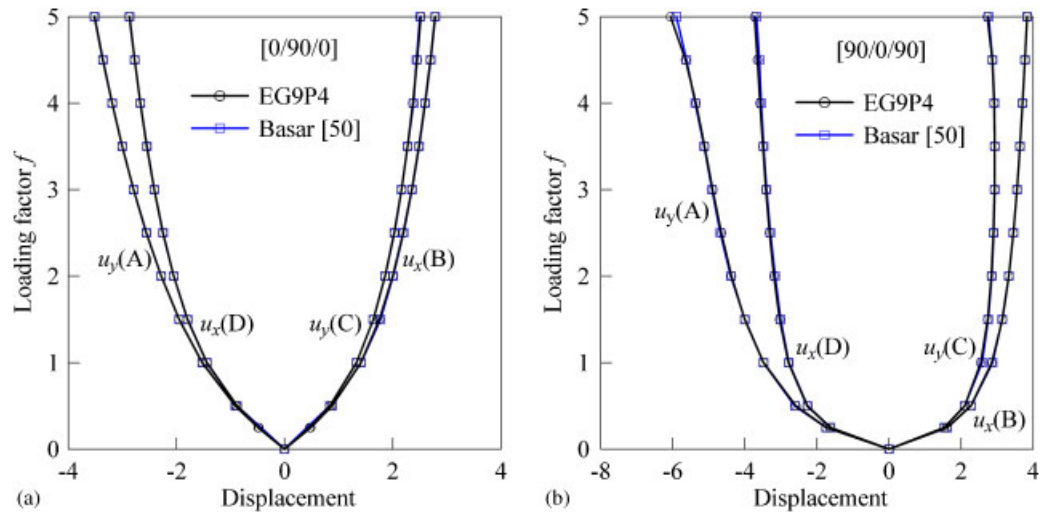
Owing to symmetry of the problem, only one octant of the shell is discretized with uniform meshes. Tables VIII and IX list displacements derived by using different EG four-node solid-shell

Table VIII. Midsurface displacements at points A and C of the $[0/90/0]$ hyperbolic shell using criterion (62) with tolerance of 10^{-4} .

Element Mesh	EG9P4 4×4	EG9P4 8×8	EG9P4 16×16	EG9P4 32×32	EG7P4 [7] 32×32	EG6P4 [7] 32×32
$-u_y(A)$	2.6075	3.3194	3.4783	3.5232	3.5217	3.5215
$u_y(C)$	2.2572	2.5515	2.5252	2.5191	2.5185	2.5179
N_{Step}/N_{Iter}	1/7	1/7	1/7	1/7	1/7	1/8

Table IX. Midsurface displacements at points A and C of the $[90/0/90]$ hyperbolic shell using criterion (62) with tolerance of 10^{-4} .

Element Mesh	EG9P4 4×4	EG9P4 8×8	EG9P4 16×16	EG9P4 32×32	EG7P4 [7] 32×32	EG6P4 [7] 32×32
$-u_y(A)$	3.1160	4.7742	5.6409	6.1325	6.1294	6.1330
$u_y(C)$	2.5376	2.9158	2.8955	2.6922	2.6932	2.6914
N_{Step}/N_{Iter}	1/10	2/14	2/20	5/26	5/25	5/29

Figure 19. Midsurface displacements of the pinched hyperbolic shell for ply orientations of: (a) $[0/90/0]$ and (b) $[90/0/90]$ (modeled by 28×28 mesh).

elements, where u_x and u_y denote the displacements of the midsurface in the x^1 - and x^2 -directions. One can observe that the EG9P4 element performs excellently because only one load step and seven Newton iterations are needed to derive a converged solution for the $[0/90/0]$ ply orientation. It is interesting to note that the EG9P4 element is the best performer in this hyperbolic shell example in spite of using 3D constitutive equations. The displacements in Figure 19 are compared additionally with the results [50], which were found employing the 28×28 mesh of finite rotation four-node degenerated-shell elements.

11. CONCLUSIONS

The simple and efficient hybrid stress–strain EG 12-node solid-shell element EG9P4 has been developed for analyses of homogeneous and laminated shells undergoing finite rotations. The finite element formulation is based on the non-linear strain–displacement relationships, which are invariant under arbitrarily large rigid-body shell motions in a convected curvilinear coordinate

system. This is due to the proposed 9-parameter shell model in which displacement vectors of S-surfaces are introduced and resolved in the reference surface frame. The developed EG solid-shell element formulation is free of assumptions of small displacements, small rotations and small loading steps. This formulation allows one to employ much larger load increments than the existing EG shell element formulations, to utilize the complete 3D constitutive equations and to analyze some 3D problems for thick composite shells with specific boundary conditions at the shell edges.

The tangent stiffness matrix is evaluated by employing 3D analytical integration and the explicit presentation of this matrix is given. The latter is unusual for the non-linear EG shell element formulation. It is noteworthy that the EG9P4 element permits the use of coarse meshes even in shell problems with extremely large displacements and rotations and it is insensitive to the number of load increments.

APPENDIX A

Herein, we briefly summarize the strain–displacement relationships for one important particular case. If the orthogonal curvilinear coordinates are referred to the lines of principal curvatures of the reference surface Ω then

$$\begin{aligned} \mathbf{a}_\alpha &= A_\alpha \mathbf{e}_\alpha, & \mathbf{a}_3 &= \mathbf{e}_3, \\ b_1^1 &= -k_1, & b_2^2 &= -k_2, & b_1^2 &= b_2^1 = 0, \\ \mu_1^{I1} &= c_1^I = 1 + k_1 z^I, & \mu_2^{I2} &= c_2^I = 1 + k_2 z^I, & \mu_1^{I2} &= \mu_2^{I1} = 0, \end{aligned} \quad (\text{A1})$$

where \mathbf{e}_i are the orthonormal base vectors of the reference surface; A_α and k_α are the coefficients of the first fundamental form and principal curvatures of the reference surface. The use of (A1) in (3) leads to

$$\mathbf{g}_\alpha^I = A_\alpha c_\alpha^I \mathbf{e}_\alpha, \quad \mathbf{g}_3^I = \mathbf{e}_3. \quad (\text{A2})$$

The displacement vectors and derivatives with respect to coordinate θ^3 at S-surfaces can be represented as follows:

$$\mathbf{u}^I = \sum_i \dot{u}_i^I \mathbf{e}_i, \quad (\text{A3})$$

$$\boldsymbol{\beta}^I = \sum_i \dot{\beta}_i^I \mathbf{e}_i, \quad (\text{A4})$$

where \dot{u}_i^I and $\dot{\beta}_i^I$ are the components of vectors \mathbf{u}^I and $\boldsymbol{\beta}^I$ in the orthonormal reference surface frame \mathbf{e}_i . Taking into account (A3) and well-known formulas for the derivatives of orthonormal vectors \mathbf{e}_i with respect to coordinates θ^α (see, e.g. [14, 25]), one derives

$$\frac{1}{A_\alpha} \mathbf{u}_{,\alpha}^I = \sum_i \lambda_{i\alpha}^I \mathbf{e}_i, \quad (\text{A5})$$

where

$$\begin{aligned} \lambda_{\alpha\alpha}^I &= \frac{1}{A_\alpha} \dot{u}_{\alpha,\alpha}^I + B_\alpha \dot{u}_\beta^I + k_\alpha \dot{u}_3^I & \text{for } \beta \neq \alpha, \\ \lambda_{\beta\alpha}^I &= \frac{1}{A_\alpha} \dot{u}_{\beta,\alpha}^I - B_\alpha \dot{u}_\alpha^I & \text{for } \beta \neq \alpha, \\ \lambda_{3\alpha}^I &= \frac{1}{A_\alpha} \dot{u}_{3,\alpha}^I - k_\alpha \dot{u}_\alpha^I, & B_\alpha = \frac{1}{A_\alpha A_\beta} A_{\alpha,\beta} & \text{for } \beta \neq \alpha. \end{aligned} \quad (\text{A6})$$

The use of (A2) in strain–displacement relationships (16) yields

$$\begin{aligned}
 2\dot{\varepsilon}_{\alpha\beta}^I &= \frac{1}{A_\alpha c_\alpha^I} \mathbf{u}_{,\alpha}^I \cdot \mathbf{e}_\beta + \frac{1}{A_\beta c_\beta^I} \mathbf{u}_{,\beta}^I \cdot \mathbf{e}_\alpha + \frac{1}{A_\alpha A_\beta c_\alpha^I c_\beta^I} \mathbf{u}_{,\alpha}^I \cdot \mathbf{u}_{,\beta}^I, \\
 2\dot{\varepsilon}_{\alpha 3}^I &= \boldsymbol{\beta}^I \cdot \mathbf{e}_\alpha + \frac{1}{A_\alpha c_\alpha^I} \mathbf{u}_{,\alpha}^I \cdot \mathbf{e}_3 + \frac{1}{A_\alpha c_\alpha^I} \boldsymbol{\beta}^I \cdot \mathbf{u}_{,\alpha}^I, \\
 2\dot{\varepsilon}_{33}^I &= 2\boldsymbol{\beta}^I \cdot \mathbf{e}_3 + \boldsymbol{\beta}^I \cdot \boldsymbol{\beta}^I,
 \end{aligned}
 \tag{A7}$$

where $\dot{\varepsilon}_{ij}^I$ are the components of the Green–Lagrange strain tensor at S-surfaces in the orthonormal reference surface frame \mathbf{e}_i . Substituting (A4) and (A5) into strain–displacement relationships (A7), we arrive at the index notations of these relationships

$$\begin{aligned}
 2\dot{\varepsilon}_{\alpha\beta}^I &= \frac{1}{c_\beta^I} \lambda_{\alpha\beta}^I + \frac{1}{c_\alpha^I} \lambda_{\beta\alpha}^I + \frac{1}{c_\alpha^I c_\beta^I} \sum_i \lambda_{i\alpha}^I \lambda_{i\beta}^I, \\
 2\dot{\varepsilon}_{\alpha 3}^I &= \dot{\beta}_\alpha^I + \frac{1}{c_\alpha^I} \lambda_{3\alpha}^I + \frac{1}{c_\alpha^I} \sum_i \dot{\beta}_i^I \lambda_{i\alpha}^I, \\
 2\dot{\varepsilon}_{33}^I &= 2\dot{\beta}_3^I + \sum_i \dot{\beta}_i^I \dot{\beta}_i^I,
 \end{aligned}
 \tag{A8}$$

where

$$\begin{aligned}
 \dot{\beta}_i^1 &= \frac{1}{h} (-3\dot{u}_i^1 + 4\dot{u}_i^2 - \dot{u}_i^3), & \dot{\beta}_i^2 &= \frac{1}{h} (-\dot{u}_i^1 + \dot{u}_i^3), \\
 \dot{\beta}_i^3 &= \frac{1}{h} (\dot{u}_i^1 - 4\dot{u}_i^2 + 3\dot{u}_i^3).
 \end{aligned}
 \tag{A9}$$

APPENDIX B

The column matrices Λ_{ijr}^I of order 36×1 introduced in Section 6 are evaluated as follows:

$$\begin{aligned}
 (\Lambda_{\alpha\alpha r}^I)_{\alpha+3I+9(s-1),1} &= d_{\alpha r s}, & (\Lambda_{\alpha\alpha r}^I)_{\beta+3I+9(s-1),1} &= \delta_{rs} B_{\alpha s} \quad \text{for } \beta \neq \alpha, \\
 (\Lambda_{\alpha\alpha r}^I)_{3+3I+9(s-1),1} &= \delta_{rs} k_{\alpha s}, \\
 (\Lambda_{\beta\alpha r}^I)_{\beta+3I+9(s-1),1} &= d_{\alpha r s}, & (\Lambda_{\beta\alpha r}^I)_{\alpha+3I+9(s-1),1} &= -\delta_{rs} B_{\alpha s} \quad \text{for } \beta \neq \alpha, \\
 (\Lambda_{3\alpha r}^I)_{3+3I+9(s-1),1} &= d_{\alpha r s}, & (\Lambda_{3\alpha r}^I)_{\alpha+3I+9(s-1),1} &= -\delta_{rs} k_{\alpha s}, \\
 (\Lambda_{i3r}^I)_{i+9(s-1),1} &= \delta_{rs} (2I-5)/h, & (\Lambda_{i3r}^I)_{3+i+9(s-1),1} &= 4\delta_{rs} (2-I)/h, \\
 (\Lambda_{i3r}^I)_{6+i+9(s-1),1} &= \delta_{rs} (2I-3)/h, \\
 d_{\alpha r s} &= \frac{1}{4\ell_\alpha A_{\alpha r}} n_{\alpha s} (1 + n_{\beta r} n_{\beta s}) \quad \text{for } \beta \neq \alpha,
 \end{aligned}$$

where $A_{\alpha r}$, $k_{\alpha r}$ and $B_{\alpha r}$ are the nodal values of the geometrical parameters of the reference surface; δ_{rs} is the Kronecker delta; parameters $n_{\alpha r}$ are defined by (32) and, as we remember, the indices r, s run from 1 to 4. The remaining components of column matrices not written out explicitly are zero.

ACKNOWLEDGEMENTS

The support of this research by the Russian Foundation for Basic Research (RFBR) under Grant No. 08-01-00373 and by the Russian Ministry of Education and Science under Grant No. 2.1./10003 is gratefully acknowledged. The authors thank the reviewers for their suggestions, which helped to improve the paper.

REFERENCES

1. Parisch H. A continuum-based shell theory for non-linear applications. *International Journal for Numerical Methods in Engineering* 1995; **38**:1855–1883.
2. Sansour C. A theory and finite element formulation of shells at finite deformations involving thickness change: circumventing the use of a rotation tensor. *Archive of Applied Mechanics* 1995; **65**:194–216.
3. Basar Y, Itskov M, Eckstein A. Composite laminates: nonlinear interlaminar stress analysis by multi-layer shell elements. *Computer Methods in Applied Mechanics and Engineering* 2000; **185**:367–397.
4. El-Abbasi N, Meguid SA. A new shell element accounting for through-thickness deformation. *Computer Methods in Applied Mechanics and Engineering* 2000; **189**:841–862.
5. Brank B. Nonlinear shell models with seven kinematic parameters. *Computer Methods in Applied Mechanics and Engineering* 2005; **194**:2336–2362.
6. Arciniega RA, Reddy JN. Tensor-based finite element formulation for geometrically nonlinear analysis of shell structures. *Computer Methods in Applied Mechanics and Engineering* 2007; **196**:1048–1073.
7. Kulikov GM, Plotnikova SV. Finite rotation geometrically exact four-node solid-shell element with seven displacement degrees of freedom. *Computer Modeling in Engineering and Sciences* 2008; **28**:15–38.
8. Lee K, Lee SW. An assumed strain solid shell element formulation with transversely quadratic displacement. *Computer Modeling in Engineering and Sciences* 2008; **34**:253–272.
9. Kulikov GM, Plotnikova SV. Calculation of composite structures subjected to follower loads by using a geometrically exact shell element. *Mechanics of Composite Materials* 2009; **45**:545–556.
10. Kim YH, Lee SW. A solid element formulation for large deflection analysis of composite shell structures. *Computers and Structures* 1988; **30**:269–274.
11. Cho C, Lee SW. On the assumed strain formulation for geometrically nonlinear analysis. *Finite Elements in Analysis and Design* 1996; **24**:31–47.
12. Kulikov GM, Plotnikova SV. Investigation of locally loaded multilayered shells by mixed finite-element method. Part II: geometrically nonlinear statement. *Mechanics of Composite Materials* 2002; **38**:539–546.
13. Sze KY, Chan WK, Pian THH. An eight-node hybrid-stress solid-shell element for geometric non-linear analysis of elastic shells. *International Journal for Numerical Methods in Engineering* 2002; **55**:853–878.
14. Kulikov GM, Plotnikova SV. Equivalent single-layer and layer-wise shell theories and rigid-body motions. Part I: foundations. *Mechanics of Advanced Materials and Structures* 2005; **12**:275–283; Part II: computational aspects 2005; **12**:331–340.
15. Kulikov GM, Plotnikova SV. Geometrically exact assumed stress–strain multilayered solid-shell elements based on the 3D analytical integration. *Computers and Structures* 2006; **84**:1275–1287.
16. Sze KY, Yao LQ. A hybrid stress ANS solid-shell element and its generalization for smart structure modelling. Part I: solid-shell element formulation. *International Journal for Numerical Methods in Engineering* 2000; **48**:545–564.
17. Buchter N, Ramm E, Roehl D. Three-dimensional extension of nonlinear shell formulation based on the enhanced assumed strain concept. *International Journal for Numerical Methods in Engineering* 1994; **37**:2551–2568.
18. Betsch P, Stein E. An assumed strain approach avoiding artificial thickness straining for a nonlinear 4-node shell element. *Communications in Numerical Methods in Engineering* 1995; **11**:899–909.
19. Kulikov GM. On the first-order seven-parameter plate theory. *Transactions of the Tambov State Technical University* 2007; **13**:518–528.
20. Kulikov GM, Carrera E. Finite deformation higher-order shell models and rigid-body motions. *International Journal of Solids and Structures* 2008; **45**:3153–3172.
21. Kulikov GM, Plotnikova SV. Non-linear strain–displacement equations exactly representing large rigid-body motions. Part II: enhanced finite element technique. *Computer Methods in Applied Mechanics and Engineering* 2006; **195**:2209–2230.
22. Wempner G, Talaslidis D, Hwang CM. A simple and efficient approximation of shells via finite quadrilateral elements. *Journal of Applied Mechanics* 1982; **49**:115–120.
23. Kulikov GM, Plotnikova SV. Non-conventional non-linear two-node hybrid stress–strain curved beam elements. *Finite Elements in Analysis and Design* 2004; **40**:1333–1359.
24. Kulikov GM, Plotnikova SV. Finite deformation plate theory and large rigid-body motions. *International Journal of Non-Linear Mechanics* 2004; **39**:1093–1109.
25. Kulikov GM, Plotnikova SV. Non-linear geometrically exact assumed stress–strain four-node solid-shell element with high coarse-mesh accuracy. *Finite Elements in Analysis and Design* 2007; **43**:425–443.
26. Kulikov GM. Strain–displacement relationships that exactly represent large rigid-body displacements. *Mechanics of Solids* 2004; **39**:105–113.
27. Hughes TJR, Tezduyar TE. Finite elements based upon Mindlin plate theory with particular reference to the four-node bilinear isoparametric element. *Journal of Applied Mechanics* 1981; **48**:587–596.
28. MacNeal RH. Derivation of element stiffness matrices by assumed strain distributions. *Nuclear Engineering and Design* 1982; **70**:3–12.
29. Bathe KJ, Dvorkin EN. A formulation of general shell elements—the use of mixed interpolation of tensorial components. *International Journal for Numerical Methods in Engineering* 1986; **22**:697–722.
30. Park KC, Stanley GM. A curved C^0 shell element based on assumed natural coordinate strains. *Journal of Applied Mechanics* 1986; **53**:278–290.

31. Pian THH. Derivation of element stiffness matrices by assumed stress distributions. *AIAA Journal* 1964; **2**: 1333–1336.
32. Pian THH, Sumihara K. Rational approach for assumed stress finite elements. *International Journal for Numerical Methods in Engineering* 1984; **20**:1685–1695.
33. Pian THH. State-of-the-art development of hybrid/mixed finite element method. *Finite Elements in Analysis and Design* 1995; **21**:5–20.
34. Lee SW, Pian THH. Improvement of plate and shell finite elements by mixed formulations. *AIAA Journal* 1978; **16**:29–34.
35. Atluri SN. On the hybrid stress finite element model for incremental analysis of large deflection problems. *International Journal of Solids and Structures* 1973; **9**:1177–1191.
36. Boland PL, Pian THH. Large deflection analysis of thin elastic structures by the assumed stress hybrid finite element method. *Computers and Structures* 1977; **7**:1–12.
37. Belytschko T, Tsay CS. A stabilization procedure for the quadrilateral plate element with one-point quadrature. *International Journal for Numerical Methods in Engineering* 1983; **19**:405–419.
38. Gruttmann F, Wagner W. A stabilized one-point integrated quadrilateral Reissner–Mindlin plate element. *International Journal for Numerical Methods in Engineering* 2004; **61**:2273–2295.
39. Batoz JL, Tahar MB. Evaluation of a new quadrilateral thin plate bending element. *International Journal for Numerical Methods in Engineering* 1982; **18**:1655–1677.
40. Timoshenko SP, Woinowsky-Krieger S. *Theory of Plates and Shells* (2nd edn). McGraw-Hill: New York, 1970.
41. Timoshenko SP, Goodier JN. *Theory of Elasticity* (3rd edn). McGraw-Hill: New York, 1970.
42. Hughes TJR, Liu WK. Nonlinear finite element analysis of shells. Part II: two-dimensional shells. *Computer Methods in Applied Mechanics and Engineering* 1981; **27**:167–181.
43. Liu WK, Law ES, Lam D, Belytschko T. Resultant-stress degenerated-shell element. *Computer Methods in Applied Mechanics and Engineering* 1986; **55**:259–300.
44. Simo JC, Fox DD, Rifai MC. On a stress resultant geometrically exact shell model. Part II: the linear theory; computational aspects. *Computer Methods in Applied Mechanics and Engineering* 1989; **73**:53–92.
45. Belytschko T, Wong BL, Stolarski H. Assumed strain stabilization procedure for the 9-node Lagrange shell element. *International Journal for Numerical Methods in Engineering* 1989; **28**:385–414.
46. Kulikov GM, Plotnikova SV. A family of ANS four-node exact geometry shell elements in general convected curvilinear coordinates. *International Journal for Numerical Methods in Engineering* 2010; **83**:1376–1406.
47. Lindberg GM, Olson MD, Cowper GR. New developments in the finite element analysis of shells. *Quarterly Bulletin of Division of Mechanical Engineering and National Aeronautical Establishment, National Research Council of Canada* 1969; **4**:1–38.
48. Kulikov GM. Refined global approximation theory of multilayered plates and shells. *Journal of Engineering Mechanics* 2001; **127**:119–125.
49. Sze KY, Liu XH, Lo SH. Popular benchmark problems for geometric nonlinear analysis of shells. *Finite Elements in Analysis and Design* 2004; **40**:1551–1569.
50. Basar Y, Ding Y, Schultz R. Refined shear-deformation models for composite laminates with finite rotations. *International Journal of Solids and Structures* 1993; **30**:2611–2638.